Journal of Medicinal Chemistry



Article

# Discovery of a New Class of Potential Multifunctional Atypical Antipsychotic Agents Targeting Dopamine D and Serotonin 5-HT and 5-HT Receptors: Design, Synthesis, and Effects on Behavior

Stefania Butini, Sandra Gemma, Giuseppe Campiani, Silvia Franceschini, Francesco Trotta, Marianna Borriello, Nicoletta Ceres, Sindu Ros, Salvatore Sanna Coccone, Matteo Bernetti, Meri De Angelis, Margherita Brindisi, Vito Nacci, Isabella Fiorini, Ettore Novellino, Alfredo Cagnotto, Tiziana Mennini, Karin Sandager-Nielsen, Jesper Tobias Andreasen, Jorgen Scheel-Kruger, Jens D. Mikkelsen, and Caterina Fattorusso

*J. Med. Chem.*, **2009**, 52 (1), 151-169 • DOI: 10.1021/jm800689g • Publication Date (Web): 15 December 2008



## More About This Article

Additional resources and features associated with this article are available within the HTML version:

- Supporting Information
- Access to high resolution figures
- Links to articles and content related to this article
- Copyright permission to reproduce figures and/or text from this article

View the Full Text HTML

# Discovery of a New Class of Potential Multifunctional Atypical Antipsychotic Agents Targeting Dopamine $D_3$ and Serotonin 5-$HT_{1A}$ and 5-$HT_{2A}$ Receptors: Design, Synthesis, and Effects on Behavior

Stefania Butini,[†,‡] Sandra Gemma,[†,‡] Giuseppe Campiani,*[,†,‡] Silvia Franceschini,[†,‡] Francesco Trotta,[†,‡] Marianna Borriello,[†,§] Nicoletta Ceres,[†,§] Sindu Ros,[†,‡] Salvatore Sanna Coccone,[†,‡] Matteo Bernetti,[†,‡] Meri De Angelis,[†,‡] Margherita Brindisi,[†,‡] Vito Nacci,[†,‡] Isabella Fiorini,[†,‡] Ettore Novellino,[†,§] Alfredo Cagnotto,[†,||] Tiziana Mennini,[†,||] Karin Sandager-Nielsen,[⊥] Jesper Tobias Andreasen,[⊥] Jorgen Scheel-Kruger,[⊥] Jens D. Mikkelsen,[#] and Caterina Fattorusso[†,§]

*European Research Centre for Drug Discovery and Development, University of Siena, Italy, Dipartimento Farmaco Chimico Tecnologico, Universitá di Siena, via Aldo Moro, 53100 Siena, Italy, Dipartimento di Chimica delle Sostanze Naturali e Dipartimento di Chimica Farmaceutica e Tossicologica, Università di Napoli Federico II, via D. Montesano 49, 80131 Napoli, Italy, Istituto di Ricerche Farmacologiche Mario Negri, Via La Masa 19, 20156 Milano, Italy, NeuroSearch A/S, Pederstrupvej 93, Ballerup DK-2750, Denmark, and Neurobiological Research Unit, University Hospital Rigshospitalet, Copenhagen, Denmark*

*Received June 6, 2008*

Dopamine $D_3$ antagonism combined with serotonin 5-$HT_{1A}$ and 5-$HT_{2A}$ receptor occupancy may represent a novel paradigm for developing innovative antipsychotics. The unique pharmacological features of **5i** are a high affinity for dopamine $D_3$, serotonin 5-$HT_{1A}$ and 5-$HT_{2A}$ receptors, together with a low affinity for dopamine $D_2$ receptors (to minimize extrapyramidal side effects), serotonin 5-$HT_{2C}$ receptors (to reduce the risk of obesity under chronic treatment), and for hERG channels (to reduce incidence of torsade des pointes). Pharmacological and biochemical data, including specific *c-fos* expression in mesocorticolimbic areas, confirmed an atypical antipsychotic profile of **5i** in vivo, characterized by the absence of catalepsy at antipsychotic dose.

## Introduction

Schizophrenia is among the most serious mental illnesses; it has a considerable social and economic impact and globally it affects approximately 1% of the world population.[1]

Antipsychotic medication is the main therapeutic intervention for schizophrenia. Although the pathophysiology of the disease has yet to be clearly defined, the development of antipsychotic drugs in recent decades has been heavily influenced by the dopamine hypothesis, mainly supported by the capability of antipsychotic drugs of interfering with dopamine receptors in vivo and in vitro and by evidence that the clinical efficacy of typical antipsychotic drugs is correlated with their occupancy at dopamine $D_2$ receptors ($D_2R$).[2]

The early agents for the treatment of psychosis, the "typical" antipsychotics (haloperidol, **1**, Chart 1), were breakthrough therapies for the positive symptoms of schizophrenia, but they failed to manage its negative symptoms and cognitive impairment. Nevertheless, typical antipsychotics carry a heavy side-effect burden (i.e., extrapyramidal symptoms (EPS) and hyperprolactinemia) and are ineffective in one-third of schizophrenic patients.[3]

The "atypical" antipsychotics (e.g., clozapine (**2**) and olanzapine (**3**)), are characterized by a multireceptor affinity profile, which combines a potent antagonism for serotonin 5-$HT_{2A}$ with a dopamine $D_2$ and $D_3$ receptors blockade.[4] Among the atypical antipsychotic agents approved by regulatory authorities, clozapine still remains invaluable for psychosis, presenting high clinical efficacy and a reduced incidence of EPS and hyperprolactinemia. Olanzapine may precipitate or unmask diabetes in susceptible patients,[5] and its use was associated with a 12% increase in excessive appetite compared to haloperidol.[6] Meanwhile, ziprasidone, risperidone, and quetiapine may be responsible for drug-induced long QT syndrome (risk of malignant ventricular arrhythmia).

A new antipsychotic agent (aripiprazole **4**, Chart 1) has recently been launched. It acts as a partial agonist at $D_2R$.[7,8] Its unique mechanism of action might underlie its efficacy and low risk of side effects seen with other antipsychotics. However, unmet clinical needs still remain and include (i) more effective antipsychotic therapy for treatment of refractory patients, (ii) improved treatment of negative symptoms, and (iii) improved treatment of cognitive dysfunction.

Several strategies for the development of novel antipsychotics have started to provide additional tools for relieving the symptoms of schizophrenia. In recent years, the pharmaceutical industry and academia have shown significant interest in the development of novel antipsychotics characterized by interaction with less obvious receptors such as metabotropic glutamate receptors and tachykinin receptors.[9]

Second-generation antipsychotics combine $D_2R$ occupancy with activity at serotoninergic receptors (such as 5-$HT_{1A}$ receptors (5-$HT_{1A}$R) and 5-$HT_{2A}$ receptors (5-$HT_{2A}$R), i.e., clozapine) to provide drug therapies for resistant schizophrenic patients, with prompter therapeutic benefits and the improvement of cognitive symptoms.[10] In contrast, we decided to exploit a novel multireceptor affinity profile approach, which combines antagonism at dopamine $D_3$ receptors ($D_3R$) and at 5-$HT_{2A}$R and partial agonism at serotonin 5-$HT_{1A}$R, with a low affinity for $D_2R$ (no liability of EPS at antipsychotic doses) and 5-$HT_{2C}$ receptors (5-$HT_{2C}$R) (reducing the risk of obesity under chronic treatment).

* To whom correspondence should be addressed. Phone: 0039-0577-234172. Fax: 0039-0577-234333. E-mail:campiani@unisi.it.
† European Research Centre for Drug Discovery and Development.
‡ Università degli Studi di Siena.
§ Università degli Studi di Napoli "Federico II".
|| Istituto Mario Negri, Milano.
⊥ NeuroSearch A/S.
# University Hospital Rigshospitalet.

10.1021/jm800689g CCC: $40.75 
Published on Web 12/15/2008

**Chart 1.** Title and Reference Compounds

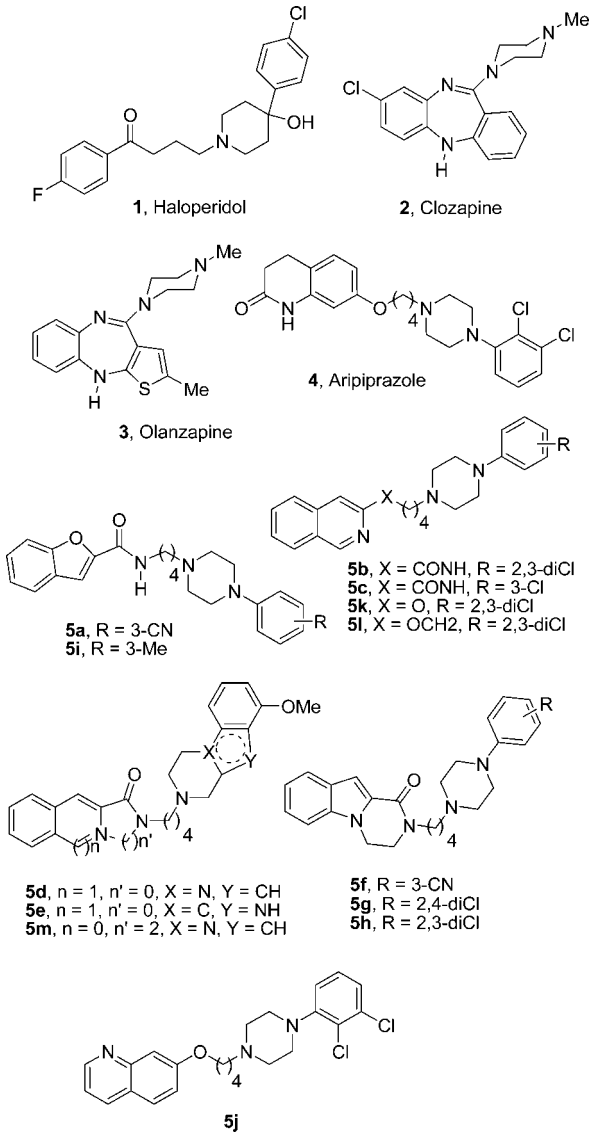


The serotoninergic system plays an important role in the regulation of prefrontal cortex (PFC) functions, including emotional control, cognitive behavior, and working memory. PFC pyramidal neurons and GABA interneurons contain several serotonin receptor subtypes with a particularly high density of 5-$HT_{1A}$R and 5-$HT_{2A}$R. It has recently been demonstrated in PFC that NMDA receptor channels are the target of 5-$HT_{1A}$R and that both receptors modulate the excitability of cortical neurons, thus affecting cognitive functions.[11] Indeed, a variety of preclinical data has suggested that the 5-$HT_{1A}$R may be a therapeutic target for the development of improved antipsychotic drugs. Although the role of 5-$HT_{1A}$R in antipsychotic drug efficacy profile remains speculative, 5-$HT_{1A}$R affinity contributes to the clinical efficacy of most of the atypical antipsychotic drugs (clozapine, olanzapine, aripiprazole) and their low liability for EPS.[12] A growing number of studies show that 5-$HT_{1A}$R activation attenuates antipsychotic-induced side effects in humans,[13] nonhuman primates,[14] and antipsychotic-induced catalepsy in rats. An association has indeed been postulated between agonist activity at 5-$HT_{1A}$R and anxiolytic or antidepressant effects, improvements in cognitive and negative symptoms, and decreased development of EPS in schizophrenia.[15] Recent studies have provided the first in vivo evidence that activation of 5-$HT_{1A}$R can play a role in aripiprazole-mediated behavior in rats.[16,17] Furthermore, because glutamatergic transmission is dysfunctional in schizophrenia and because glutamate release is decreased by 5-$HT_{1A}$R activation,[18] agonist properties at postsynaptic 5-$HT_{1A}$R may be relevant to the therapeutic profile of atypical antipsychotic agents, improving negative symptoms and cognitive deficits. This topic has recently been reviewed by Meltzer and Sumiyoshi,[19] who underline the additional beneficial effects found in many preclinical models based on the reciprocal interaction with the 5-$HT_{1A}$R (agonists) and 5-$HT_{2A}$R (antagonists). Serotonin, through its interaction with 5-$HT_{2A}$R, inhibits neuronal activity in the substantia nigra and ventral tegmental area. 5-$HT_{2A}$R antagonists may increase the firing rate of midbrain dopaminergic neurons in a state-dependent manner and potentiate the increase in the activity of nigrostriatal dopamine-containing neurons in response to moderate $D_2$R antagonism by antipsychotics. Therefore, 5-$HT_{2A}$R antagonism may prevent or alleviate EPS induced by acute or long-term treatment with typical drugs such as **1**.

Although the role of dopamine $D_2$R and serotonin 5-$HT_{2A}$R has been defined, the role of $D_3$R is still controversial. Recently, $D_3$R has been claimed as a potential target for antischizophrenic drug development.[20] This is mainly based on the specific distribution of $D_3$Rs in the mesolimbic dopaminergic system, along with the observation of elevated levels of these receptors in patients that are off antipsychotics. $D_3$R functions are primarily related to the mesolimbic, rather than the nigrostriatal, dopaminergic system, thus the blockade of $D_3$R does not elicit EPS. Furthermore, because dopamine through $D_3$R modulates the cholinergic system at the prefrontal cortex level, $D_3$R antagonists (devoid of muscarinic effects) may robustly enhance acetylcholine release in frontal cortex.[21] Consequently, $D_3$R antagonists might improve cognitive deficits poorly treated by currently available agents, including clozapine. The persistent concern is whether selective $D_3$R blockade can relieve positive symptoms of schizophrenia. Investigation of dopamine $D_3$R function was limited because of the lack of highly selective ligands.

To validate the novel approach to antipsychotics and to achieve an optimum interaction with dopamine and serotonin receptors, we exploited our knowledge acquired in the development of tricyclic atypical antipsychotics.[22] Thus, we selected the arylalkylpiperazine system as a flexible scaffold for achieving a fine balancing of dopamine $D_3$R and serotonin 5-$HT_{1A}$R and 5-$HT_{2A}$R affinity, reducing $D_1$R, $D_2$R, and 5-$HT_{2C}$R occupancy. Starting from highly selective $D_3$R hits[23] that lack significant behavioral effects, the present article deals with the design, synthesis, and behavioral investigation of a rationally designed set of arylpiperazines as novel and potent antipsychotics, characterized by high affinity for $D_3$R, 5-$HT_{1A}$R, and 5-$HT_{2A}$R. Their structure−activity relationships (SARs) for dopamine and serotonin receptors were associated with variation of the aromatic system and the substituents on the arylpiperazine moiety. Among the analogues synthesized and tested (**5a**−**m**), compound **5i**, a selective antagonist at $D_3$R and 5-$HT_{2A}$R, and partial agonist at 5-$HT_{1A}$R, was selected for further biological investigation. Its atypical antipsychotic profile is herein discussed, together with the molecular modeling study. Despite its structural similarity to aripiprazole (nanomolar affinity for $D_2$R, $D_3$R, 5-$HT_{1A}$R, and 5-$HT_{2A}$R, Table 2), **5i** shows a unique pharmacological profile, being designed to validate the novel approach to atypical antipsychotics based on a $D_3$, 5-$HT_{1A}$, and 5-$HT_{2A}$ multireceptor affinity profile.

**Table 1.** Physical and Chemical Data for Compounds **5a−m**

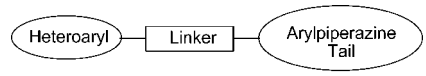


**5a-m**

| Cpd | Heteroaryl | Linker | Arylpiperazine Tail | Yield%[a] | mp (°C) | Formula | Anal[c] |
|---|---|---|---|---|---|---|---|
| **5a** | 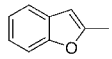 | $CONH(CH_2)_4$ | 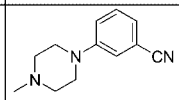 | 90.0 | oil | $C_{24}H_{26}N_4O_2$ | C,H,N |
| **5b** | 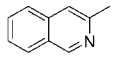 | $CONH(CH_2)_4$ | 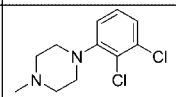 | 60.2 | oil | $C_{24}H_{26}Cl_2N_4O$ | C,H,N |
| **5c** | 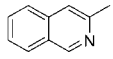 | $CONH(CH_2)_4$ | 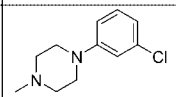 | 50.4 | 156-157[b] | $C_{24}H_{27}ClN_4O$ | C,H,N |
| **5d** | 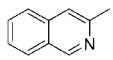 | $CONH(CH_2)_4$ | 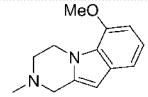 | 55.0 | oil | $C_{26}H_{28}N_4O_2$ | C,H,N |
| **5e** | 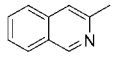 | $CONH(CH_2)_4$ | 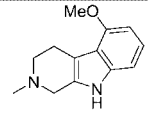 | 30.0 | oil | $C_{26}H_{28}N_4O_2$ | C,H,N |
| **5f** | 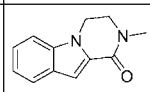 | $(CH_2)_4$ | 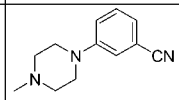 | 60.0 | oil | $C_{26}H_{29}N_5O$ | C,H,N |
| **5g** | 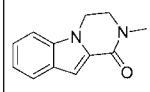 | $(CH_2)_4$ | 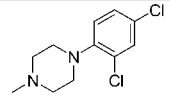 | 87.4 | oil | $C_{25}H_{28}Cl_2N_4O$ | C,H,N |
| **5h** | 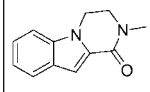 | $(CH_2)_4$ | 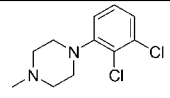 | 78.2 | 160-161[b] | $C_{25}H_{28}Cl_2N_4O$ | C,H,N |
| **5i** | 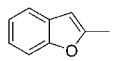 | $CONH(CH_2)_4$ | 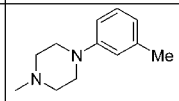 | 52.0 | 119-120[b] | $C_{24}H_{29}N_3O_2$ | C,H,N |
| **5j** | 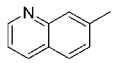 | $O(CH_2)_4$ | 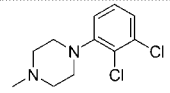 | 62.4 | oil | $C_{23}H_{25}Cl_2N_3O$ | C,H,N |
| **5k** | 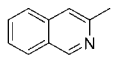 | $O(CH_2)_4$ | 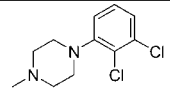 | 61.0 | Amorphous solid | $C_{23}H_{25}Cl_2N_3O$ | C,H,N |
| **5l** | 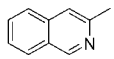 | $O(CH_2)_5$ | 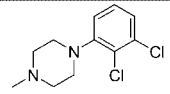 | 54.3 | 133-134[b] | $C_{24}H_{27}Cl_2N_3O$ | C,H,N |
| **5m** | 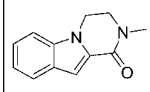 | $(CH_2)_4$ | 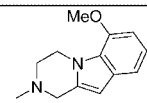 | 62.0 | oil | $C_{27}H_{30}N_4O_2$ | C,H,N |

[a] Yields refer to isolated and purified materials. [b] Recrystallization solvent: methanol. [c] All the compounds were analyzed within ±0.4% of the theoretical values.

Furthermore, long QT syndrome, experienced with several antipsychotics, has prompted considerable efforts in trying to define the molecular basis of this phenomenon. Consequently, efforts to predict long QT syndrome risk have been focused on assays testing hERG channel activities. Investigation of hERG channel blockade is now a key step along the drug discovery trajectory of the pharmaceutical industry. Therefore, hERG channel interaction was introduced as a further parameter in our design strategy of the novel antipsychotics.

**Table 2.** Binding Affinities for $D_1$, $D_2$, $D_3$, 5-$HT_{1A}$, 5-$HT_{2A}$, and 5-$HT_{2C}$ Receptors ($K_i$ nM ± SD)[a] and hERG Channels ($K_i$ $\mu$M) of Compounds **5a**−**m** and Reference Antipsychotics

| compd | $D_1$[b] | $D_2$[c] | $D_{3r}$[d] | 5-$HT_{1A}$[e] | 5-$HT_{2A}$[f] | 5-$HT_{2C}$[g] | hERG[h] |
|---|---|---|---|---|---|---|---|
| **5a** | >10000 | 859 ± 121 | 0.54 ± 0.07 | 876 ± 22 | NT[i] | NT[i] | 0.39 (2) |
| **5b** | 4600 ± 870 | >10000 | 0.099 ± 0.002 | 5.0 ± 0.3 | 41 ± 5 | 136 ± 25 | 0.20 (3) |
| **5c** | 5500 ± 1130 | 1039 ± 190 | 0.27 ± 0.02 | 14.7 ± 0.6 | 23.4 ± 6 | 173 ± 23 | 0.30 (4) |
| **5d** | >10000 | 1012 ± 29 | 33.5 ± 3.5 | 28.0 ± 1.3 | 164 ± 12 | 1086 ± 190 | 1.84 (2) |
| **5e** | >10000 | 6475 ± 646 | 6.0 ± 0.5 | 118 ± 16 | 149 ± 39 | 434 ± 47 | NT[i] |
| **5f** | >10000 | 339 ± 86 | 3.7 ± 0.5 | NT[i] | 389 ± 34 | NT[i] | NT[i] |
| **5g** | 4315 ± 880 | 229 ± 76 | 3.2 ± 0.4 | NT[i] | 300 ± 63 | NT[i] | NT[i] |
| **5h** | 4370 ± 852 | 122 ± 37 | 0.105 ± 0.002 | 9.3 ± 1.9 | 83 ± 28 | 18.4 ± 3.0 | 0.20 (4) |
| **5i** | 3290 ± 418 | 263 ± 31 | 4.5 ± 0.8 | 11.9 ± 1.7 | 15.3 ± 3.2 | 206 ± 14 | 0.93 (2) |
| **5j** | NA[j] | 63 ± 6 | 8.2 ± 0.9 | 4.0 ± 0.7 | 127 ± 28 | NT[i] | NT[i] |
| **5k** | NT[i] | 215 ± 15 | 32.92 ± 3 | 24.2 ± 2 | 122.76 ± 15 | NT[i] | 0.16 (2) |
| **5l** | 7124 ± 488 | 75 ± 7 | 0.14 ± 0.03 | 18.0 ± 4.3 | 57 ± 11 | 154 ± 14 | 0.21 (2) |
| **5m** | >10000 | 3530 ± 918 | 8.6 ± 0.9 | 33 ± 3 | 200 ± 40 | 1360 ± 191 | 0.26 (2) |
| **1** | 318 ± 22 | 2.6 ± 0.5 | 0.9 ± 0.04 | 1800 ± 310 | 164 ± 88 | 4700 ± 500 | 0.12 (8) |
| **2** | 353 ± 67 | 210 ± 31 | 319 ± 55 | 160 ± 30 | 10 ± 2 | 4.8 ± 0.4 | 17 (3) |
| **3** | 25 ± 3.5 | 20 ± 17 | 39 ± 5.9 | 610 ± 85 | 4.0 ± 1.0 | 4.1 ± 0.9 | 36 (2) |
| **4** | 1960 ± 180 | 0.8 ± 0.07 | 3.3 ± 0.5 | 5.6 ± 0.2 | 8.7 ± 0.9 | 22 ± 1.7 | 1.02 (2) |
| Risperidone | 50 ± 2 | 3.8 ± 0.3 | 6.7 ± 0.7 | 190 ± 15 | 0.15 ± 0.02 | 32 ± 2.2 | 0.92 (2) |

[a] Each value is the mean ± SD of three determinations and represents nM $K_i$ value. [b] [$^3$H]SCH 23390, rat striatum. [c] [$^3$H]spiperone, rat striatum. [d] [$^3$H]-7-OH-DPAT, Sf9 cells. [e] [$^3$H]-8-OH-DPAT, rat hippocampus. [f] [$^3$H]ketanserin, rat cortex. [g] [$^3$H]mesulergine, guinea pig cortex. [h] Each value is the mean of 2−8 determinations (number of determinations are given in parentheses), SD were all within 10% of the mean. [i] NT not tested. [j] NA not active at 100 $\mu$M.

**Table 3.** Multiple Sequence Alignment of the Trans-Membrane Ligand-Binding Domain of Considered Human DAR and 5-HTR Subtypes

| TM1−7 similarity (%) | receptor subtype | TM2 sequence[a,b] | TM3 sequence[a,b] | TM4 sequence[a,b] | TM5 sequence[a,b] | TM6 sequence[a,b] | TM7 sequence[a,b] |
|---|---|---|---|---|---|---|---|
| | $D_3$ | LVMP**W**VVV**Y**L | FVTL**D**VMMC | ITAV**W**VLA**F** | FVIY**S**S**V**V**S**FYLP | FI**V**C**W**LP**FF**L | SA**T**T**W**LG**Y**V |
| 81 | $D_2$ | LVMP**W**VVV**Y**L | FVTL**D**VMMC | ISIV**W**VLS**F** | FVVY**S**S**I**V**S**FYVP | FI**I**C**W**LP**FF**I | SA**F**T**W**LG**Y**V |
| 63 | 5-$HT_{2C}$ | LVMPLSLLA | WISL**D**VLFS | IAIV**W**AISI | FVLI**G**S**F**V**A**FFIP | FL**I**M**W**CP**FF**I | NV**F**V**W**IG**Y**V |
| 61 | 5-$HT_{1A}$ | LVLPMAALY | FIAL**D**VLCC | ISLT**W**LIG**F** | YTIY**S**T**F**G**A**FYIP | FI**L**C**W**LP**FF**I | AI**I**N**W**LG**Y**S |
| 59 | 5-$HT_{2A}$ | LVMPVSMLT | WIYL**D**VLFS | IIAV**W**TISV | FVLI**G**S**F**V**S**FFIP | FV**V**M**W**CP**FF**I | NV**F**V**W**IG**Y**L |
| 57 | $D_1$ | LVMP**W**KAVA | WVAF**D**IMCS | ISVA**W**TLSV | YAIS**S**S**V**I**S**FYIP | FVCC**W**LP**FF**I | DVF**V**W**F**G**W**A |

[a] Bold: conserved Asp residue on TM3, serine residues on TM5, and aromatic residues lining the ligand binding pocket. [b] Underlined: residues displayed in Figure 1A,C.

## Chemistry

The synthesis of compounds **5a**−**m** (Chart 1 and Table 1) is described in the Schemes 1−4.

The secondary amine synthons **8** and **13** were synthesized following the synthetic strategies described in Schemes 1 and 2. Compound **8** was prepared starting from previously described ethyl 7-methoxyindole-2-carboxylate **6**,[24] which was *N*-alkylated with bromoacetonitrile to afford the cyano-derivative **7**.[25] Reduction of nitrile **7** using an excess of lithium aluminum hydride gave rise to a cyclic lactam intermediate that was further reduced in situ to afford the target amine **8**.[25]

The synthesis of the known $\beta$-carboline **13** was realized by a modification of the literature procedure[26] as described in Scheme 2. Formylation of the indole-derivative **9** at C3 was performed using *N*-chlorosuccinimide (NCS), triphenylphosphine, and *N*,*N*-dimethylformamide (DMF).[27] The aldehyde **10** thus obtained was treated with nitromethane and ammonium acetate to afford 4-methoxy-3-(2-nitrovinyl)-1*H*-indole **11**.[28] This latter was subsequently reduced by lithium aluminum hydride, and the corresponding tryptamine derivative **12** was submitted to a classic Pictet−Spengler reaction, affording the $\beta$-carboline **13**.[26]

**Scheme 1.** Synthesis of Intermediate **8**

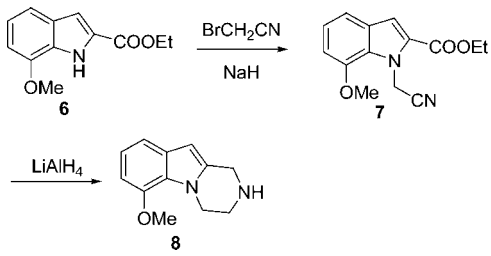


**Scheme 2.** Synthesis of Intermediate **13**

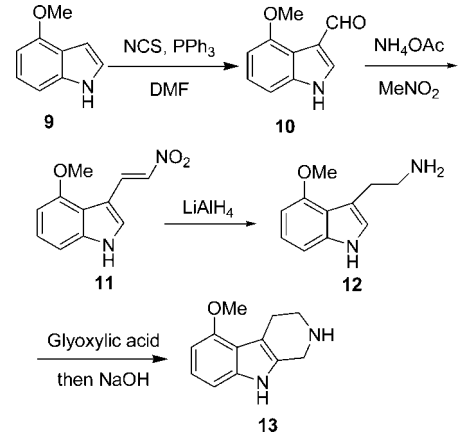


The synthetic pathway for obtaining compounds **5a**−**i**,**m** is shown in Scheme 3. The bromo-derivatives **14a**,**b** and **15** were obtained according to the procedure previously reported in the literature.[23] Subsequent alkylation of suitable arylpiperazines (commercially available, or obtained by a previously reported methodology,[23] or according to Schemes 1 and 2) gave the final compounds **5a**−**i**,**m**.

The ether-derivatives **5j**−**l** (Scheme 4) were synthesized starting from the aromatic hydroxy-derivatives **16a**,**b**, which were *O*-alkylated with the appropriate commercially available dibromoalkane in the presence of cesium carbonate as a base.

**Scheme 3.** Synthesis of Compounds **5a–i**,m

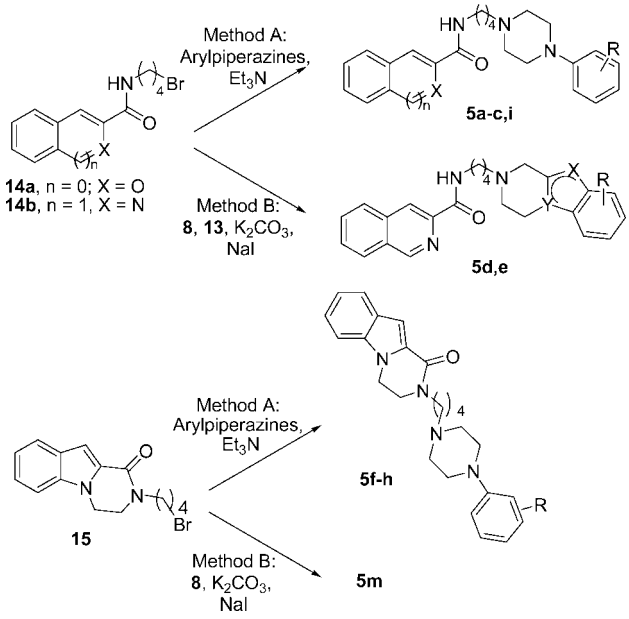


**Scheme 4.** Synthesis of Compounds **5j−l**

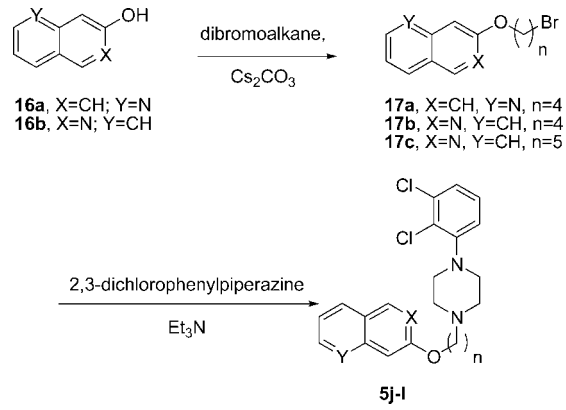


The bromo-derivatives **17a**−c were reacted with 2,3-dichlorophenylpiperazine to give compounds **5j**−**l**.[23]

## Results and Discussion

For in vitro and in vivo testing, compounds **5a**−**m** were used as mono-, di-, or trihydrochloride salts.

The binding affinities for 5-$HT_{1A}$, 5-$HT_{2C}$, 5-$HT_{2A}$, $D_1$, $D_2$, and $D_3$ receptors of compounds **5a**−**m**, together with clozapine, olanzapine, and haloperidol, are given in Table 2. Furthermore, Table 2 lists the affinity of the tested compounds for hERG channels. Figure 3 summarizes the effects of **5i** in animal models sensitive to mesolimbic mediated antipsychotic activity (methamphetamine (MAMP)) and phencyclidine (PCP) induced hyperactivity) and striatal mediated side effects (catalepsy). Figure 4 reports the effect of **5i** on Fos protein induction in the nucleus accumbens shell subregion, and core subregion and in the dorsolateral part of the rostral striatum. Table 4 reports a summary of the behavioral effects of **5c**, **5h**, 5**i**, **5l**, and the reference compounds.

**1. Rational Design, Binding Studies, and Structure−Activity Relationships (SARs). Design Strategy.** The challenge in designing new potential antipsychotics is to balance, in a single molecular structure, the required activity and selectivity toward specific multiple receptor subtypes (multireceptor affinity profile). We had previously acquired experience in tricyclic antipsychotics[22] and in arylpiperazines designed to selectively interact with $D_3$R to modulate cocaine-seeking behavior.[23] In this work, we therefore decided to exploit specific modifications of the versatile arylpiperazine scaffold. We were following an innovative pharmacological hypothesis aimed at modulating activity toward highly homologous dopamine receptors, such as $D_2$R and $D_3$R, while still maintaining a good affinity for serotonin 5-$HT_{1A}$ and 5-$HT_{2A}$ receptors and minimizing affinity for the $D_1$R and 5-$HT_{2C}$R subtypes. Furthermore, to improve the drugability of the novel antipsychotics, we directed our design strategy at limiting hERG potassium channel inhibition by up to 1 $\mu$M, thus minimizing the risk of long QT syndrome and cardiac side effects.

To drive the structural modifications of this new series of arylpiperazine derivatives, we performed a conformational and electronic analysis of the ligands, along with a structural and bioinformatic analysis of the above-mentioned serotonin and dopamine receptor subtypes (see Experimental Section for details). The amino acid (AA) sequences of the receptors were aligned[29] with the aim of mapping their active sites' homology and a model of the putative binding site for our competitive ligands was produced (Homology, Insight2005, Accelrys, San Diego) (Table 3, Figure 1A,C). Indeed, all the considered receptors (i.e., $D_1$, $D_2$, $D_3$, 5-$HT_{1A}$, 5-$HT_{2A}$, and 5-$HT_{2C}$) belong to the 7tm_1 family of G-protein coupled receptors (GPCRs). In particular, the two endogenous aromatic amines, dopamine and serotonin, share a homologous binding site.[30] Many GPCRs models have been proposed, derived from analogies with high-resolution structures of rhodopsin. Despite this, the actual seven trans-membrane (TMs) helices connectivity, arrangement, and 3D structure in the different GPCR subtypes is still unknown. However, biophysical and mutagenesis studies on rhodopsin and a number of ligand-activated GPCRs provided evidence that the formation of the receptor active state involves movements of TM5, TM6, and TM7 with respect to TM3.[31−34] In particular, different clusters of aromatic residues, critical to receptor structure and ligand recognition, were identified.[31,35,36] The very recently solved structure of the $\beta_2$-adrenergic receptor in complex with the inverse agonist carazolol[37−39] confirmed the data obtained from mutagenesis studies[35] and offered a new template for the generation of receptor 3D models (see Experimental Section).

The generated receptor models provided the rational bases for driving structural modification of the arylpiperazine skeleton in order to achieve the desired dopamine/serotonin receptor subtype selectivity. Consequently, we first identified, in the arylpiperazine skeleton, different pharmacophoric moieties (Chart 2) aimed at binding to the corresponding interaction sites identified in different secondary structures of the receptor models (Figure 1). In this view, the polymethylene tether length is crucial for guaranteeing the required structural flexibility in order to adapt the different pharmacophoric moieties to multiple receptors' binding sites. Indeed, in agreement with the reported structural and biochemical data on dopamine and serotonin receptors, we hypothesized that our competitive ligands bind by placing their heteroaromatic moiety (namely the "head") into the "relevant aromatic pocket"[22c] formed by the motif $W_i$, $F_{i+3}$, $F_{i+4}$ on the TM6 helix, which is conserved throughout the biogenic amine receptors (Table 3, Figure 1).[35,38] At the same time, the H-bonding group of our compounds is thought to interact with the equally conserved Ser/Thr residues on TM5 helix, reported to be important for receptor interaction/activation as well as for ligand specificity (see the discussion below for

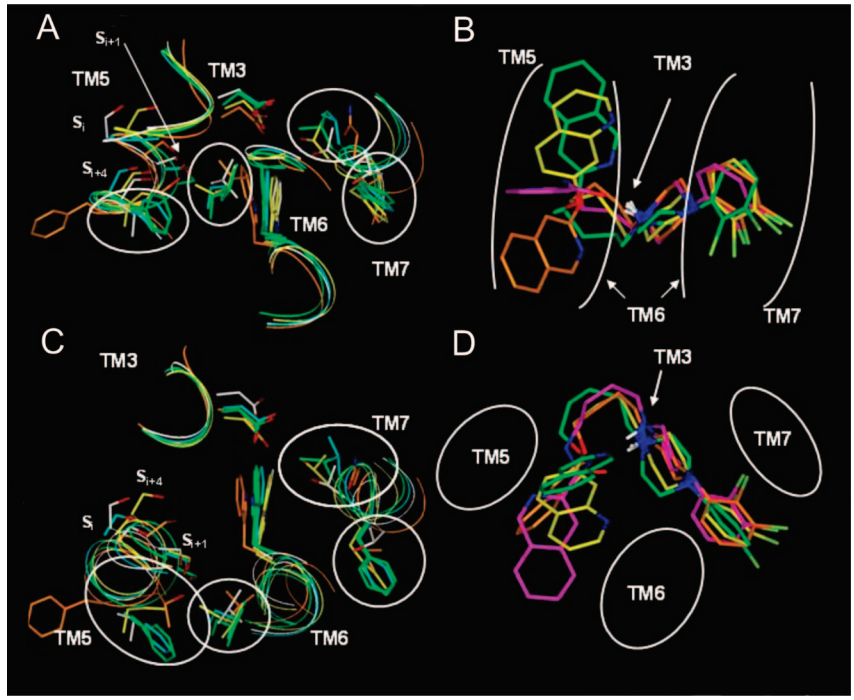


**Figure 1.** Binding sites (A: longitudinal view; C: transversal view) of 5-HTR and DAR 3D models. The inactive state (template: $\beta_2$ adrenergic receptor; PDB code: 2RH1) of $D_2R$ (yellow), $D_3R$ (white), 5-$HT_{2A}R$ (cyan), and 5-$HT_{2C}R$ (green), and the active state (template: bovine rhodopsine; PDB code: 2I37) of 5-$HT_{1A}R$ (orange) are superimposed by Cα atoms. Key residues on TM3, TM5, TM6, and TM7 are displayed. AA involved in subtype selectivity are highlighted by white circles. Serine residues on TM5 are labeled as discussed in the main text. Longitudinal (B) and transversal (D) view of **5b** (magenta), **5j** (yellow), **5k** (orange), and **5l** (green) AM1 global minimum conformers, superimposed by fitting their pharmacophoric moieties (i.e., "head" ring centroid; protonated piperazine nitrogen hydrogen; H-bond donor group; "tail" ring centroid). The hypothesized interactions with TM3, TM5, TM6, and TM7 receptor helices are evidenced.

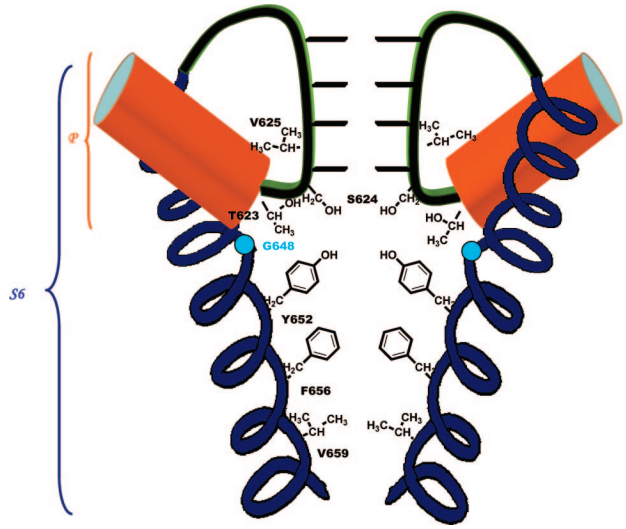


**Figure 2.** Illustrated representation of the central pore cavity of hERG channels according to the model reported by Stansfeld et al.[46] The central pore helix P and the S6 helix are indicated by orange and blue brackets, respectively. Key binding residues for blockers identified by mutagenesis studies are evidenced.

details).[31,40] Finally, the Asp residue on TM3, present in all GPCRs amine receptors, is likely to interact with the protonated piperazine nitrogen of our ligands (Table 1 and 3, Figure 1). Moreover, because the binding sites of both dopamine and serotonin contain additional aromatic pockets, modification of the chemical-physical features of the "tail" of our compounds could drive the molecule to assume alternative binding modes in the active site, adapting (or not) to different receptor subtypes. Indeed, in addition to the above-mentioned Trp residue on TM6, all the considered receptors have in common a further Trp residue on TM4 and TM7 helices (dopamine subtypes also on TM2), lining the substrate binding site (Figure 1A,C and Table 3). Mutagenesis studies in the 5-$HT_{2A}R$ also support an interaction of serotonergic ligands with the conserved Trp on TM7.[41] However, crucial changes in the AA composition of dopamine and serotonin binding sites determine the molecular bases for substrate and ligand selectivity (Figure 1 and Table 3). In particular, residues that are critical for pharmacological specificity are often one turn of helix away from the critical "conserved" residues.[35,38]

Hence, taking into account the structural homology among our dopamine and serotonin receptor models, as well as the structural comparison with other known dopamine/serotonin competitive ligands, we rationally modified the electronic and conformational features of our ligands on the basis of our experience in the field of antipsychotics[22] and in the development of selective $D_3R$ ligands.[23] Accordingly, we maintained the 4-methylene linker in the amide series of compounds, because it was previously demonstrated to be the optimal spacer for high $D_3R$ affinity,[42] while we tested 4- and 5-methylene linkers in the ether series (**5j**−**l**, Table 1). However, we varied the chemical-physical parameters of: (i) the heteroaromatic system at the "head", (ii) the functional group (X) connecting the "head" to the methylene linker, (iii) the phenyl ring at the "tail", by modifying the nature, position, and number of substituents (Chart 2 and Table 1).

Following this rationale, we were able to obtain the optimal affinity profile for entering into further in vivo experiments.

**Dopamine Receptors.** According to dopamine receptors' classification ($D_1$-like and $D_2$-like subfamilies), dopamine $D_1R$ showed the lowest degree of sequence homology with both $D_2R$ and $D_3R$, and with 5-HTRs, presenting relevant AA changes in

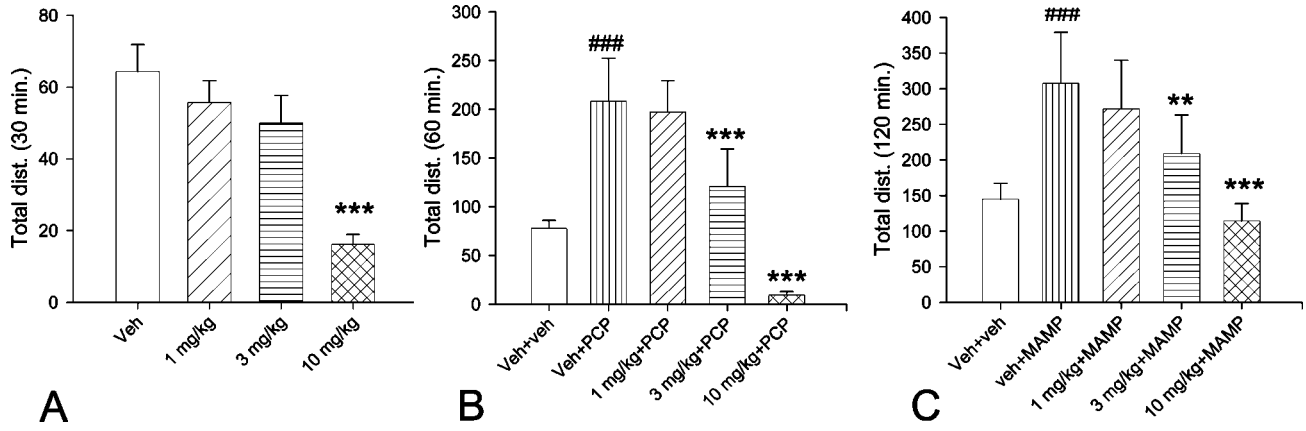


**Figure 3.** Effect of compound **5i** on spontaneous exploratory locomotor activity (A), MAMP (B), and PCP-induced hyperactivity (C). (A) Compound **5i** caused a dose-dependent reduction in spontaneous exploratory locomotor activity, marginally reducing activity at 3 mg/kg ($p < 0.05$) and potently reducing activity at 10 mg/kg ($p < 0.001$). (B) Compound **5i** dose-dependently reduced MAMP-induced hyperactivity in doses of 3 and 10 mg/kg when compared to VEH + MAMP ($p < 0.01$ and $p < 0.001$ respectively). (C) Likewise, PCP-induced hyperactivity was also significantly reduced by compound **5i**, reaching statistical significance at 3 and 10 mg/kg ($p < 0.001$ for both) when compared to VEH + PCP. $n = 7$ pr dose group. Results are expressed as means ± SEM of distance traveled. Statistical evaluation was performed by two-way ANOVA followed by Tukey test for multiple comparisons. ###: $p < 0.001$ versus vehicle treatment; **: $p < 0.01$ versus MAMP/PCP treatment; ***: $p < 0.001$ versus MAMP/PCP treatment.

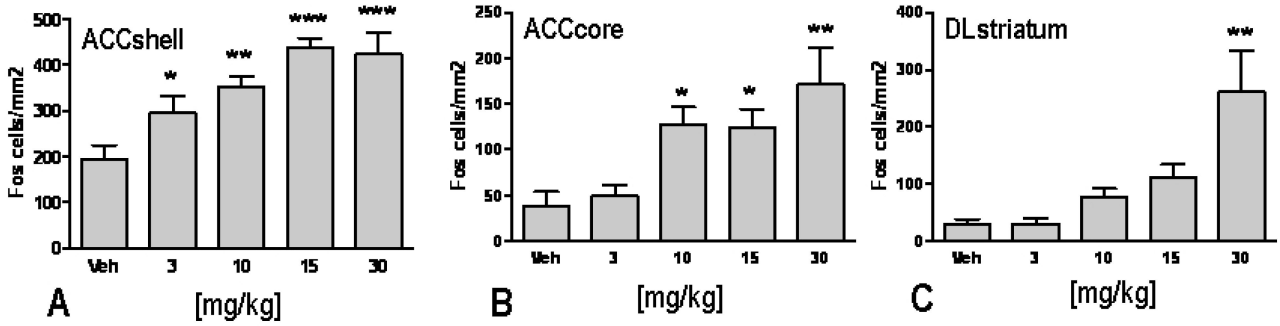


**Figure 4.** Effect of a single intraperitoneal dose of **5i** on Fos induction 60 min after the treatment in the nucleus accumbens shell subregion (A), the nucleus accumbens core subregion (B), and the dorsolateral part of the rostral striatum (C). The results are expressed as means ± SEM of the number of Fos-immunoreactive cells/mm$^2$ in all regions. *$P < 0.05$, **$P < 0.01$, ***$P < 0.001$ when compared to respective vehicle-treated group.

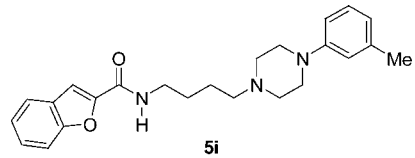


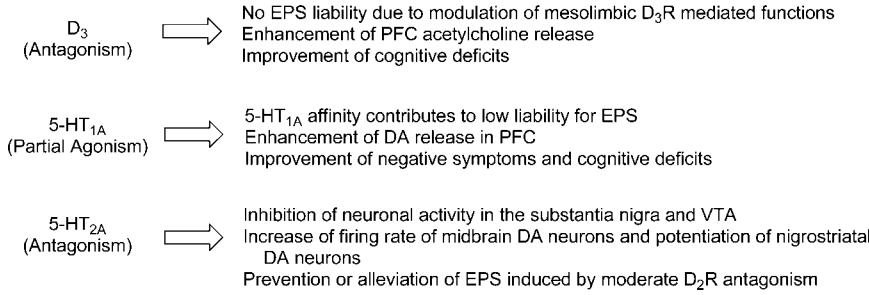


**Figure 5.** Outline of **5i** multireceptor affinity profile and its significance for optimizing the atypical antipsychotic profile.

TM1, TM2, TM5, TM6, and TM7 helices involved in ligand−receptor interaction/activation (Table 3).[35,40] Accordingly, we easily designed arylpiperazines devoid of $D_1$R affinity (Table 2). However, despite the high degree of identity between $D_2$R and $D_3$R active sites, we were able to selectively modulate $D_2$R occupancy in our series of compounds.

The $D_2$R and $D_3$R substrate binding site both present on TM2, TM4, and TM7 helices, an aromatic residue placed one turn of helix away (i.e., at the i+3/i+4 position) with respect to the conserved Trp residue, thus forming additional aromatic pockets (Table 3). Nevertheless, on $D_3$R TM7 helix, there is a Thr residue, not conserved in $D_2$R, just before the conserved Trp

**Table 4.** Summary of Behavioral Effects of **5c**, **5h**, **5i**, and **5l** Compared to the Effects of **18**, **19**, Aripiprazole, Clozapine, and Haloperidol Tested Under Identical Conditions

| compd | expl. locom.[a] $ED_{50}$ (mg/kg) | MAMP locom.[b] $ED_{50}$ (mg/kg) | PCP locom.[c] $ED_{50}$ (mg/kg) | catalepsy |
|---|---|---|---|---|
| **5c** | 14 | 4.2 | 6.7 | |
| **5h** | >30 | 3.7 | >3 | |
| **5i** | 5.5 | 2.1 | 2.6 | >30 |
| **5l** | >30 | >10 | >10 | |
| **18** | | | >30 | |
| **19** | | | >30 | |
| Aripiprazole | 0.6 | <0.3 | 0.2 | >30 |
| Clozapine | 2.4 | 2.5 | 1.1 | >30 |
| Haloperidol | 0.08 | 0.06 | 0.09 | 0.19 |

[a] Expl. Locom.: exploratory locomotor activity; [b] MAMP locom.: methamphetamine-induced locomotor activity; [c] PCP locom.: PCP-induced locomotor activity.

**Chart 2.** General Structure of Title Compounds

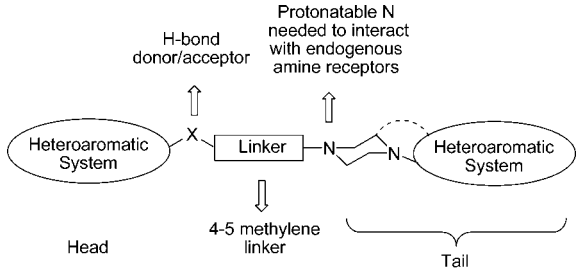


**Chart 3.** Structure and Binding Profile of Compounds **18** and **19**

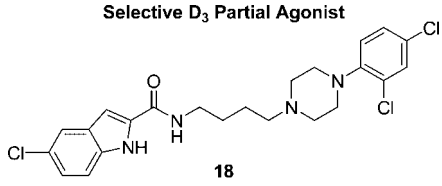


**18**

$Ki_{D3}$ = 0.38 nM
$Ki_{D2}$ and $Ki_{5\text{-}HT1A}$ > 10000 nM

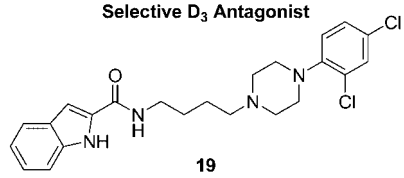


**19**

$Ki_{D3}$ = 0.18 nM
$Ki_{D2}$ and $Ki_{5\text{-}HT1A}$ > 10000 nM

residue (T369, human $D_3$ numbering; Table 3). This could offer a further H-bond interaction site (i.e., besides the Ser stretch $S_i$, $S_{i+1}$, $S_{i+4}$ on TM5) close to the relevant aromatic pocket on TM6 and the Asp residue on TM3 (Figure 1A,C). Consequently, the arylpiperazine skeleton is suitable for high $D_3R$ affinity, likely placing (i) the protonated *N* in contact with the Asp residue on TM3, (ii) the heteroaromatic "head" (Chart 2) on the relevant aromatic pocket on TM6, establishing H-bond interactions with TM5 or TM7, and (iii) the aromatic "tail" in one of the additional aromatic pockets on TM2, TM4, and TM7 (Figure 1). It cannot be excluded that significant structural changes in the molecule, such as the introduction of further H-bond donor/acceptor groups at the "tail", could drive this latter into the relevant aromatic pocket on TM6, leading to putative additional binding modes.[22c] To this end, we succeeded in maintaining high $D_3R$ affinity through the whole series of compounds (Table 2).

The crucial role in $D_2R/D_3R$ selectivity played by the orientation of H-bond donor/acceptor group(s) (supposed to interact with the serine stretch $S_i$, $S_{i+1}$, $S_{i+4}$ on TM5) with respect to the extra volume occupied by the heteroaromatic ring (supposed to contact TM6) (Figure 1) was already observed by us,[23] and it is confirmed by the affinity profile of the newly designed compounds (Table 2). In fact, when an ether function (X = O) is replaced by an amide bond (X = CONH) (Charts 1, 2 and Table 1), $D_2R$ affinity dramatically decreased and the compound become extremely selective toward $D_3R$ (**5k** vs **5b**, Table 2). Indeed, in addition to the above-mentioned Thr residue on TM7, $D_2R$ and $D_3R$ present further differences in the AA composition of their binding site. In particular, in the hydrophobic cleft between TM5 and TM6, bulky Ile residues are present in $D_2R$ (I195(TM5) and I391(TM6), human numbering; Figure 1, Table 3), while at the $D_3R$ level, these isoleucines are replaced by the less hindered Val residues. This may account for the potency and selectivity of the designed compounds toward $D_3R$. Accordingly, the different amino acid composition of the regions shaped between TM5/TM6 and TM6/TM7 helixes was exploited by us to obtain the desired $D_3R/D_2R$ selectivity profile by modifying the "head" of title compounds, (Chart 2, Tables 1−3, Figure 1A−D). In particular, the electronic partial charge distribution of **5j**−**l**, in their AM1 global minimum conformer (Figure 1B,D), evidenced the bridging oxygen (full optimized AM1 partial charge = −0.26) and the heteroaromatic nitrogen (full optimized AM1 partial charge ∼−0.20) lone pairs as putative H-bond acceptor groups. Our computational analysis also highlighted that the high flexibility due to the ether linker (i.e., at least five $sp^3$ atoms), together with the formation of an H-bond interaction between the electron-dense ether oxygen (conjugated to an heteroaromatic ring) and the protonated piperazine nitrogen (Figure 1B,D), strongly stabilized a "butterfly-shaped" conformation, fitting the $D_2R$ pharmacophoric requirements reported for tricyclic $D_2R$ antagonists.[22c] Thus, the ether derivatives may be able to: (i) interact with the serine stretch $S_i$, $S_{i+1}$, $S_{i+4}$ on TM5, (ii) accommodate the heteroaromatic "head" in the region between TM5 and TM6 establishing favorable interactions with the relevant aromatic pocket on TM6 ($W_i$, $F_{i+3}$, $F_{i+4}$ motif), (iii) interact with the Asp residue on TM3, and (iv) place the "tail" in the additional aromatic pocket on TM7 (Figure 1). Because the flexibility of the alkyl tether determines the disposition of the pharmacophoric moieties, it plays a key role in dopamine receptors (DAR) affinity.[23] In the present series, this is confirmed by the ether derivative **5l** (**5l** vs **5k**, Figure 1B,D, Table 1, 2). However, when an amide bond is in place (**5b**), our calculations revealed the occurrence of intramolecular H-bonds between: (i) the amide hydrogen and the isoquinoline nitrogen, and (ii) the carbonyl oxygen and the protonated piperazine nitrogen. Accordingly, we calculated a strong conformational preference for this family of "H-bonded" conformers. In consequence, the amide derivatives are characterized by a different orientation of the heteroaromatic "head" with respect to the H-bonding groups (Chart 2, Figure 1B,D). Indeed, in the case of the amide bridged analogues, the carbonyl oxygen (full optimized AM1 partial charge = −0.46), the aromatic heteroatom (full optimized AM1 partial charge ∼−0.15), and the amide hydrogen (partial charge = 0.26) represent the most probable H-bond donor/acceptor to interact with the above-mentioned serine stretch on TM5 helix (Figure 1). To establish this latter interaction and, at the same time, to accommodate the heteroaromatic "head" in the "relevant aromatic pocket" on

TM6, the molecule should project toward the above-mentioned hydrophobic region between TM5 and TM6, where bulky Ile residues are present in $D_2R$ (Figure 1, Table 3). This may account for the very low affinity of **5b** vs **5k/5l**. According to these observations, the conformationally constrained analogues **5f** and **5h**, lacking the H-bond acceptor group (NH), proved to be more potent than **5a** and **5b** on $D_2R$, although the potency on $D_3R$ was comparable (Table 2).

Once we had selected the amidic function at the "head" (X group, Chart 2) to get the best affinity pattern at $D_2R$ and $D_3R$, we explored the influence of specific substitutions at the "tail" level in order to obtain the desired pharmacological profile. On the basis of our previous findings,[23] different electron withdrawing groups were introduced on the phenyl ring at the "tail" to lower $D_2R$ affinity (Table 1). Among the arylpiperazines tested in the present series, the 2,3-dichlorophenyl piperazine (**5b**, **5g**, **5h**, **5j**−**l**) provided analogues with significant $D_2R$ occupancy and the best $D_3R$ affinity. However, they differed, as predicted, in the $D_2R/D_3R$ affinity ratio by 1−5 orders of magnitude (Table 2). By shifting the *meta*-chlorine atom at the *para* position, the affinity decreased on both subtypes, although this effect was more pronounced on $D_3R$ than on $D_2R$ (**5h** vs **5g**, Table 2). Contrary to the trend previously observed for $D_2R$ on chlorine-substituted arylpiperazines,[23] the introduction of electron-withdrawing substituents at the *meta* position of the phenyl ring increased $D_3R$ affinity (**5a** vs **5i**, Table 2). On these bases, compound **5i**, bearing a methyl group at the *meta* position, despite showing a decreased $D_3R$ receptor affinity with respect to **5a**, still maintained a great selectivity profile, exhibiting, in addition, low affinity for hERG channel (see below).

Finally, in agreement with our design hypothesis, the $D_3R$ binding site can tolerate significant structural changes. In particular, according to the presence of T198 on TM7, which may allow alternative binding modes, introducing further H-bonding groups at the "tail" of the arylpiperazine skeleton (i.e., compounds **5d**, **5e**, and **5m**) we maintained good $D_3R$ affinity and $D_2R/D_3R$ selectivity ratios.

**Serotonin Receptors.** 5-$HT_{1A}R$ affinity is not greatly influenced by the position of the H-bonding group at the "head" of the arylpiperazine skeleton (Chart 2, Table 2). Indeed, compounds **5b**,**c**, **5h**−**j**, and **5l**, characterized by different heteroaromatic moieties and X groups (Chart 2, Table 1), presented a 5-$HT_{1A}R$ affinity ranging from 5.0 to 18.0 nM (Table 2). However, the affinity of the above-cited set of compounds on 5-$HT_{2A}R$ (ranging from 15.3 to 127 nM, Table 2) demonstrated the different sensitivity of the two serotonin receptor subtypes to structural modifications at the "head" of our arylpiperazine scaffold. Similarly, the variation of the alkyl tether length in the ether series differently affected serotonin receptor subtype affinity (**5l** vs **5k**, Tables 1 and 2). In fact, these serotonin receptor subtypes present critical AA changes in the TM5 helix (Figure 1A,C, Table 3), which can account for the observed SARs.[34,43,44] In particular, the DAR serine stretch ($S_i$, $S_{i+1}$, $S_{i+4}$) on TM5 is not conserved in 5-$HT_{1A}R$, where $S_i$ is still present, but $S_{i+1}$ and $S_{i+4}$ are replaced by a Thr and an Ala residue, respectively. In contrast, in the 5-$HT_{2A}R$ subtype $S_i$ is replaced by a Gly residue, while $S_{i+1}$ and $S_{i+4}$ are conserved (Table 3).

Moreover, 5-$HT_{1A}R$ binding site presents an Asn residue on TM7 (N386, human 5-$HT_{1A}R$ human numbering, Table 3), corresponding to the $\beta$-adrenergic receptor TM7 Asn residue involved in carazolole binding.[37−39] As with $D_3R$ (reported above), this could represent a putative additional H-bond interaction site besides the Ser stretch on TM5 (Figure 1A,C). It could also allow in 5-HTR subtypes alternative binding modes for the arylpiperazine-like skeleton.

The intrinsic activity showed by compound **5i** (see next paragraph) indicated an agonist like effect on 5-$HT_{1A}R$ only. Interestingly, in the activated state of GPCRs (Figure 1 protein orange), TM5 turns clockwise, shifting one residue away. Although in 5-$HT_{1A}R$ $S_{i+1}$ is missing, the clockwise shifting during the receptor activation pushes the $S_i$ serine residue (conserved in 5-$HT_{1A}R$) to occupy the $S_{i+1}$ serine position of the inactivated state. The position of the $S_{i+1}$ serine residue of the inactivated state now corresponds to the position of the $S_i$ serine residue of the activated state (Figure 1A,C). Thus **5i** binds 5-$HT_{1A}R$ in the activated state. This observation may explain the intrinsic activity of **5i** at 5-$HT_{1A}R$.

The higher tolerance of 5-$HT_{2A}R$ with respect to $D_2R$ has already been evidenced and exploited by us in the design of new atypical antipsychotics based on a tricyclic scaffold.[22] It is noteworthy that the pharmacophoric requirements reported to be responsible for $D_2R/5\text{-}HT_{2A}R$ selectivity in the tricyclic series, such as the distance between the aromatic ring binding to the relevant aromatic pocket on TM6 and the protonated nitrogen binding to TM3, are similarly related to the selectivity profile of our new arylpiperazine-like derivatives (e.g., **5b**, distance = 7.42 Å, $K_{iD2}$ > 10000 nM, $K_{i5\text{-}HT2A}$ = 41 nM vs **5j**, distance = 5.63 Å, $K_{iD2}$ = 63 nM, $K_{i5\text{-}HT2A}$ = 127 nM).

The analogues **5b**−**e**, **5h**,**i**, and **5l**,**m** were also tested on 5-$HT_{2C}R$. Of these, only the indole-based ligand **5h**, characterized by the presence of alkyl-substituted nitrogens at the "head" of the structure (Table 1), showed a significant affinity ($K_i$ = 18.4 nM, Table 2). Accordingly, in 5-$HT_{2C}R$ only $S_{i+1}$ is conserved, while $S_i$ and $S_{i+4}$ are replaced by a Gly and an Ala residue, respectively. Moreover, bulky hydrophobic residues are present around $S_{i+1}$ on TM5 and TM6 (Table 3, Figure 1). Biochemical studies[4,34,46] demonstrated that mutation of these residues causes a substantial alteration of ligand specificity and selectivity.

In conclusion, we based our design strategy on the differences among receptor subtypes' composition of TM5/6/7 helices. We have thus been able to design compounds with weak affinity for 5-$HT_{2C}R$ while maintaining the desired affinity and activity profile on 5-$HT_{1A}R$ and 5-$HT_{2A}R$.

Following our rationale, the optimal dopamine/serotonin receptors' affinity balance was obtained for compounds **5b**, **5c**, and **5i** (Table 2) characterized by: (i) the isoquinoline (**5b** and **5c**) or benzofurane (**5i**) rings as heteroaromatic systems (Table 1), (ii) the amide bond as X group, and (iii) the presence of small electron-withdrawing (**5b** and **5c**) and/or -donating (**5i**) substituents at 2 and/or 3 phenyl ring position of the arylpiperazine moiety.

**Ether-a-gogo-Related Gene (hERG) KC Channels.** Reducing the risk of drug-induced cardiac arrhythmia is recognized as a major hurdle in the successful development of new drugs. To date, investigation of hERG channel blockade has been a significant step along the drug discovery trajectory of the pharmaceutical industry. The most common problem is acquired long QT syndrome. This is caused by drugs that block human ether-a-gogo-related-gene (hERG) KC channels, delay cardiac repolarization, and increase the risk of torsades de pointes arrhythmia (TdP). Indeed, efforts to predict long QT syndrome risk have been focused on assays testing hERG channel activities. This is because hERG channel blockade is an important indicator of potential pro-arrhythmic liability. Drug-induced arrhythmia by noncardiac drugs is rare. However, commonly used medications can induce ventricular arrhythmia.

These include antipsychotics, antimalarials, and antidepressants. Although these drugs represent different therapeutic classes and chemical structures, they share the ability to prolong the QT interval, which is an indirect measure of ventricular-repolarization time measured from the ECG and a known risk factor for TdP. Sertindole and thioridazine were recently withdrawn from the market for this reason.

To date, long QT syndrome has alarmed regulatory authorities and has been most often associated with drug-induced ventricular arrhythmia. We therefore believe that weeding out potential hERG channel blocker activity as early as possible, preferably in the drug-design stage, will eliminate a lot of safety concerns that have previously accompanied the development of numerous drugs, especially antipsychotics. To this end, we decided to investigate hERG channel interaction at the earliest stages of the drug design and discovery process. Starting from the published protein-based and ligand-based pharmacophore models (hERG cartoon at Figure 2), we exploited our experience in drug design and, consequently, developed our own strategy for the structural class of compounds under investigation.

Scanning alanine mutagenesis studies have identified key binding-sensitive residues for a growing list of known hERG blockers in the inner helix (S6) and in the loop connecting S6 to the pore helix, close to the potassium selectivity filter.[47−50] In particular, the binding site of drugs blocking hERG functionality is contained within the central pore cavity of the pore domain, located below the selectivity filter and flanked by the four S6 helices of the tetrameric channel. Ligand-binding sensitivity to Ala mutations has been demonstrated for (i) T623, S624, and V625 residues, at the base of the selectivity filter and for (ii) G648, Y652, F656, and V659 residues, all of which lie on the same face of S6 helix (i, i + 4 positions) (Figure 2).

All potent hERG blockers are highly sensitive to Y652A and F656A mutations. The presence of these two aromatic amino acids (Y652 and F656) in S6 of hERG is unique to the ether-a-go-go family of $K^+$ channels. Indeed, despite the lack of negative charged residue on the hERG S6 inner helix, the binding of the cationic species is guaranteed by the overall negative electrostatic field inside the hERG cavity. This is due to Tyr and Phe side chains lining the inner pore in a 4-fold symmetry. However, the tetrameric assembling of the S6 and pore helices suggests the possibility of alternative binding modes for blockers. This is also supported by data obtained from mutagenesis studies.[51] Therefore, hERG pore structure can account for the observed unintentional binding of biogene amine competitive agonists/antagonists, such as antipsychotics. Accordingly, published hERG blockers pharmacophores[52,53] share similar features with the dopamine/serotonin pharmacophores, consisting of two or more hydrophobic/aromatic groups surrounding a basic center. Thus, it is not surprising that our arylpiperazine derivatives showed blocking properties on hERG, although at high nanomolar concentrations (Table 2). Our strategy, to lower hERG affinity to the micromolar level, was based on the principle that, although hERG channels and dopamine/serotonin receptors share a similar and highly polarized binding site for cationic species (reflected in the similarity of the predicted hERG blockers and antipsychotics pharmacophores), the polarization of the endogenous ligand and, consequently, the polarization of the active site itself, must differ. Accordingly, once we had established the key pharmacophoric features necessary for obtaining the desired receptor binding profile, we tried to modulate hERG affinity by changing the polarization of the phenyl group at the "tail" of the compounds. This strategy led to the discovery of **5i**, a potential atypical antipsychotic agent characterized by low affinity for hERG (Table 2).

Following this approach, we have been able to modulate hERG channel occupancy within the same structural class of compounds while maintaining the desired receptor binding profile (**5a** vs **5b** and **5i**, Tables 1 and 2) and in vivo pharmacological properties.

**Miscellaneous Receptor Binding and 5i Intrinsic Activity at Selected Receptors.** On the basis of its unique binding profile, **5i** was therefore tested against a panel of other receptors including histamine $H_1$ receptors ($K_i$ = 15 nM), central imidazole $I_2$ receptors ($K_i$ = 138 nM) and adrenergic receptors $\alpha_1$ and $\alpha_2$ ($K_i$ of 6 and 43 nM, respectively). The affinity for alpha receptors is a critical aspect of clozapine/olanzapine binding profile. The $\alpha_2$ or 5-$HT_{1A}$R[54] occupancy might explain the marked increase in dopamine output in the prefrontal cortex induced by clozapine, which is beneficial to cognitive functions. The $\alpha_2$ affinity of **5i** might enhance its clinical efficacy, while its $\alpha_1$ occupancy might protect against dopamine deficits.

The intrinsic activity of compound **5i**, at $D_{2L}$, $D_{2S}$, and $D_3$ receptors was determined in [$^{35}$S]-GTP$\gamma$S binding assays, at 5-$HT_{2A}$R was determined in rat aortic ring contraction model, and at 5-$HT_{1A}$R in guinea pig ileum relaxation model. Compound **5i** behaves as antagonist at $D_{2L}$ receptors ($IC_{50}$ = 584 nM), at $D_{2S}$ receptors ($IC_{50}$ = 1240 nM), and at $D_3$R ($IC_{50}$ = 143 nM). On 5-$HT_{2A}$R, **5i** displayed antagonist-like effects ($IC_{50}$ = 230 nM), while on 5-$HT_{1A}$R displayed agonist like effects ($IC_{50}$ = 180 nM).

Taking into account the great potency of **5i** on serotonin, dopamine, and adrenergic receptors, this compound, together with **5c**,**h**,**k**, was selected as a promising atypical antipsychotic agent and subjected to in vivo pharmacological characterization.

**2. Behavioral Studies. 2.1. Can Selective $D_3$R Blockade Relieve Positive Symptoms?** To validate the approach herein proposed for the treatment of schizophrenia, the first question to be addressed was whether selective $D_3$R occupancy alone relieves positive symptoms of schizophrenia. Previously, we reported the synthesis of the arylpiperazines **18** and **19** (Chart 3) designed to investigate the role of $D_2$R/$D_3$R on cocaine-seeking behavior.[23] Arylpiperazines **18** and **19** proved to be two of the most potent and selective $D_3$R ligands showing partial agonist properties (**18**) or full antagonism (**19**) toward $D_3$R.[23] Both compounds were used in the present study as pharmacological tools to investigate the role played by $D_3$R occupancy on schizophrenia models. They did not show significant behavioral effect in the animal models herein described.

Together with the arylpiperazine aripiprazole (**4**), an analogous arylpiperazine characterized by high potency against $D_2$R, $D_3$R, 5-$HT_{1A}$R, and 5-$HT_{2A}$R, compounds **18** and **19** were tested in the PCP-induced hyperactivity animal model for psychosis. While aripiprazole showed a dose-dependent reduction of hyperactivity (Table 4), compounds **18** and **19** did not significantly reduce hyperactivity ($ED_{50}$ > 30 mg/kg, Table 4), indicating that $D_3$R occupancy alone lacks efficacy in animal models predictive for antipsychotic properties. We concluded that $D_3$R selective ligands may not relieve positive symptoms of schizophrenia. Accordingly, we designed arylpiperazines capable of interacting with $D_3$R, 5-$HT_{1A}$R, and 5-$HT_{2A}$R.

**2.2. Behavioral Effects of a Selected Set of Novel Arylpiperazines.** An initial behavioral screening was performed on compounds **5c**, **5h**, **5i**, and **5l**, selected on the basis of their multireceptor affinity profile. Clinically, the term "atypical antipsychotic" has been used for drugs, like clozapine, that

relieve positive symptoms at doses that do not cause side effects such as prolactin increase and extrapyramidal effects. Preclinically, this translates into drugs that show effect in models of psychosis at doses that do not cause dopamine $D_2R$ related side effects. In this study, side-effect liability was evaluated by the horizontal bar test, which is very sensitive for catalepsy induced by dopamine $D_2R$ blockade. Antipsychotic potential of the compounds was assessed in mice rendered hyperactive by MAMP and PCP. Both tests are sensitive to mesolimbic mediated antipsychotic activity. Meth- (or D-) amphetamine-induced hyperactivity are potently reduced by $D_2R$ antagonists, such as haloperidol, whereas PCP-induced hyperactivity has been reported to be more sensitive to atypical antipsychotic compounds when compared to typical antipsychotics.[55]

**2.3. Effects of 5c, 5h, 5i, 5l, and Reference Compounds on Spontaneous Exploratory Locomotor Activity.** In the exploratory locomotor activity test, the mice are transferred to new cages immediately before the test began and consequently used the first 30 min or so to explore their new environment. Compounds that cause sedation or induce motor disturbances will result in reduction in spontaneous exploratory locomotor activity. Pretreatment with 3, 10, and 30 mg/kg of compound **5h** and **5l** only mildly reduced exploratory locomotor activity with $ED_{50}$ values >30 mg/kg (Table 4). Compounds **5c** and **5i** dose-dependently reduced spontaneous locomotor activity with $ED_{50}$ values at 13.8 and 5.5 mg/kg, respectively (Table 4, and Figure 3 for **5i**). For comparison, aripiprazole, clozapine, and haloperidol were tested. All three compounds reduced exploratory locomotor activity with $ED_{50}$ values of 0.6, 2.4, and 0.08 mg/kg, respectively.

**2.4. Effects of 5c, 5h, 5i, and 5l on Methamphetamine-Induced Locomotor Activity.** As shown in Table 4 and Figure 3 for **5i**, pretreatment with 1, 3, and 10 mg/kg of compound **5l** did not reduce MAMP-induced hyperactivity when compared to MAMP alone ($ED_{50}$ value >10 mg/kg). In contrast, pretreatment with 1, 3, and 10 mg/kg of compounds **5c**, **5h**, and **5i** all caused a dose-related reduction in MAMP-induced hyperactivity, with $ED_{50}$ values of 4.2, 3.7, and 2.1 mg/kg, respectively. These effects cannot be accounted for by drug-induced sedation because sedative effects were only observed in the exploratory locomotor activity test at $ED_{50}$ values ranging from 2.6- to 8.1-fold higher doses (see above). For comparison, aripiprazole, clozapine, and haloperidol were also tested. All three compounds dose-dependently reduced MAMP-induced hyperactivity. Aripiprazole reduced MAMP-induced hyperactivity with $ED_{50}$ < 0.3 mg/kg, i.e., at least 2-fold lower than the $ED_{50}$ value for sedative effects in the exploratory locomotor activity test ($ED_{50}$ = 0.6 mg/kg). Clozapine reduced MAMP-induced hyperactivity with $ED_{50}$ = 2.5 mg/kg, which was in the same dose range as needed to cause sedation in the exploratory locomotor test ($ED_{50}$ = 2.4 mg/kg). Haloperidol reduced MAMP-induced hyperactivity with $ED_{50}$ = 0.06 mg/kg, also in the same dose range as needed to cause sedation ($ED_{50}$ = 0.08 in exploratory locomotor activity). Accordingly, compounds **5c**, **5h**, and **5i** showed a favorable profile when compared to both atypical and typical reference compounds in this test, with a 2−8 fold separation between doses causing sedation and doses reducing MAMP-induced hyperactivity.

**2.5. Effects of Compounds 5c, 5h, 5i, and 5l on PCP-Induced Locomotor Activity.** Pretreatment with 0.3, 1, and 3 mg/kg of compound **5h** and 1, 3, and 10 mg/kg of compound **5l** was not able to reduce PCP-induced increase in locomotor activity ($ED_{50}$ > 3 and > 10 mg/kg, respectively). In contrast, compounds **5c** and **5i**, both dosed in 1, 3, and 10 mg/kg, dose-dependently reduced hyperactivity induced by PCP with $ED_{50}$ values at 6.7 and 2.6 mg/kg, respectively. Sedative effects were observed at approximately 2-fold higher $ED_{50}$ values in the exploratory locomotor activity test (13.8 mg/kg for compound **5c** and 5.5 mg/kg for compound **5i**). The atypical antipsychotic compounds aripiprazole and clozapine both dose-dependently reduced PCP-induced hyperactivity. Aripiprazole was administered at doses of 0.1, 0.3, and 1 mg/kg and inhibited PCP-induced hyperactivity with an $ED_{50}$ value of 0.2 mg/kg. Clozapine, dosed in 0.3, 1, and 3 mg/kg, reduced PCP-induced hyperactivity with an $ED_{50}$ value of 1.1 mg/kg. Both compounds showed sedative effects in the exploratory locomotor activity test with $ED_{50}$ values approximately twice the $ED_{50}$ values necessary to reduce PCP-induced hyperactivity. Furthermore, the typical antipsychotic compound haloperidol, tested at doses of 0.01, 0.025, and 0.05 mg/kg, reduced PCP-induced hyperactivity, reaching $ED_{50}$ at 0.09 mg/kg. This is in the same dose range as the $ED_{50}$ for causing sedation in the exploratory locomotor activity test ($ED_{50}$ = 0.08 mg/kg). In summary, compounds **5c** and **5i** both showed favorable profiles in MAMP- and PCP-induced hyperactivity when compared to typical as well as atypical antipsychotic reference compounds (Table 4, and Figure 3 for **5i**). On the basis of these results, **5i** was selected as the lead compound of the new series and was subjected to side-effect evaluation to further characterize its atypical antipsychotic profile.

**2.6. Comparison of Cataleptogenic Effects of Aripiprazole, Clozapine, Haloperidol and Compound 5i.** Compound **5i** did not cause catalepsy in the horizontal bar test at doses up to 30 mg/kg (Table 4). As expected, the typical antipsychotic compound haloperidol dose-dependently resulted in catalepsy with an $ED_{50}$ value of 0.19 mg/kg, while the atypical antipsychotic compounds aripiprazole and clozapine did not induce catalepsy at doses up to 30 mg/kg.

**2.7. Mesocorticolimbic Selectivity and Atypical Antipsychotic Profile of 5i.** The immunochemistry of the Fos protein has been shown to be useful in mapping functional pathways in the central nervous system and especially in identifying brain areas that are targets for antipsychotics. Moreover, the ability of these drugs to increase Fos protein expression in the striatal complex has been considered useful in discriminating between typical and atypical antipsychotic compounds.[56] In contrast to haloperidol, but like most atypical antipsychotics, **5i** did not affect Fos immunoreactivity in the regions implicated in the control of extrapyramidal motor function, such as the dorsolateral striatum. However, like clozapine, it markedly enhanced the expression of Fos protein in the mesocorticolimbic regions, which are involved in the control of affective and motivational behaviors, i.e., the shell subregion of the nucleus accumbens (Figure 4). In this respect, **5i** clearly behaves as an atypical antipsychotic. However, it is worth noting that not all of the atypical antipsychotics, which similarly increase Fos expression in limbic areas, can enhance this expression in the medial prefrontal cortex too.[56a]

A single systemic injection of **5i** produced a dose-dependent and site-selective induction of the transcription factor Fos in the limbic striatum (Figure 4). There were clear topographical differences in the induction of Fos in different striatal areas. While **5i** markedly increased the number of Fos-immunoreactive cells in the nucleus accumbens (ACC) ACCshell at a dose of 3 mg/kg, higher doses were necessary to produce an induction in the ACCcore and an even higher in the dorsolateral (DL) DLstriatum (Figure 4). In the ACCcore, **5i** had no effect at a low dose, but at 10 mg/kg and higher, the compound induced

Fos in this region. Similarly, in the DLstriatum, **5i** increased the Fos induction, but only at the extremely high dose of 30 mg/kg.

Interestingly, it has been recently shown[57] that the 5-$HT_{1A}$R agonist 8-OH-DPAT is able to convert the "typical" pattern of haloperidol on *c-fos* expression into a pattern resembling that of clozapine, suggesting that the profile of Fos protein expression of **5i** might be linked to partial agonist properties at 5-$HT_{1A}$R.

**3. Summary of the in Vivo Characterization of the Atypical Antipsychotic Agent 5i and Its Therapeutic Potential.** As already discussed, **5i** (1, 3, 10 mg/kg, sc) caused a dose-dependent reduction in MAMP- and PCP- induced hyperactivity in mice, reaching $ED_{50}$ values of 2.1 and 2.6 mg/kg, respectively. In the exploratory locomotor activity test, sedation was only observed with $ED_{50}$ values approximately twice the value needed to reduce psychostimulant-induced hyperactivity. This is in the same range observed in this study by marketed atypical antipsychotics such as aripiprazole and clozapine. The ratio between $ED_{50}$ for reducing MAMP-/PCP-induced hyperactivity and $ED_{50}$ for sedation ranges between 1 and 3. $D_2$R-related side-effects liability was evaluated by the horizontal bar test. Neither compound **5i** nor aripiprazole nor clozapine caused catalepsy up to the highest dose tested (30 mg/kg). In contrast, haloperidol potently induced catalepsy with an $ED_{50}$ value of 0.19 mg/kg. In conclusion, **5i** has an approximate 200-fold selectivity toward the $D_3$R ($K_{iD2}$ = 764 nM; $K_{iD3}$ = 4.5 nM) and high affinity for 5-$HT_{1A}$R and 5-$HT_{2A}$R with ($K_i$ = 12 and 15 nM, respectively). Taking this into account, **5i** was found effective in psychosis models without showing effect in the striatal-mediated side-effect models, suggesting antipsychotic activity with no propensity for causing $D_2$R-related side effects.

The in vivo studies, after acute administration of **5i**, clearly showed that this compound has an antipsychotic potential. As with all other antipsychotics tested so far, **5i** induces Fos in the nucleus accumbens shell.[58,59] Furthermore, **5i** displays an atypical profile, activating neurons exclusively in the limbic/ventral striatal subdivisions rather than the sensory-motor portions in the dorsolateral striatum.

## Conclusions

In summary, starting from highly potent and selective dopamine $D_3$R ligands previously described, with no overt behavioral effects in animal model for schizophrenia, we discovered novel arylpiperazine atypical antipsychotic agents characterized by specific occupancy of $D_3$R, 5-$HT_{1A}$R, and 5-$HT_{2A}$R. Interaction with $D_2$R and 5-$HT_{2C}$R was minimized in order to reduce any liability of EPS and to reduce the risk of obesity under chronic treatment, respectively. The analogue **5i**, which has unique receptor affinity properties on dopamine, serotonin, and adrenergic receptors, was identified as a potential atypical drug candidate. The binding profile of **5i** suggests a complex interaction on the cortical receptors involved in the regulation of the activity of prefrontal cortical cells innervated by ventral tegmental area neurones (5-$HT_{2A}$, dopaminergic, and α adrenergic receptor subtypes). Moreover, **5i** showed a low affinity for hERG channels. **5i** validated the hypothesis based on specific interaction with $D_3$R, 5-$HT_{1A}$R, and 5-$HT_{2A}$R for the discovery of innovative antipsychotic drugs (Figure 5). **5i** reduced methamphetamine as well as PCP-induced locomotor activity without causing catalepsy (up to 30 mg/kg, sc). Moreover, $ED_{50}$ for reducing MAMP- and PCP-induced hyperactivity was approximately a factor 2-fold lower than the $ED_{50}$ for causing sedation. This was found to be in the same range for the two marketed atypical antipsychotics, aripiprazole and clozapine. Accordingly, **5i** shows an "atypical" antipsychotic activity without liability for side effects as measured by standard behavioral testing paradigms. This is supported by the preferred increase in expression of Fos immunoreactive cells in the ACCshell when compared to ACCcore and DLstriatum. Moreover, the data would suggest a therapeutic index of at least 10−15-fold between efficacy (methamphetamine or PCP models) and side effects (catalepsy). These findings indirectly illustrate the high and selective activity of **5i** toward the mesolimbic and mesocortical dopaminergic system. **5i** may pave the way for the development of a novel class of drugs for the treatment of neuropsychiatric disorders.

## Experimental Section

Reagents were purchased from Aldrich and were used as received. Reaction progress was monitored by TLC using Merck silica gel 60 $F_{254}$ (0.040−0.063 mm) with detection by UV. Merck silica gel 60 (0.040−0.063 mm) was used for column chromatography.

Melting points were determined in Pyrex capillary tubes using an Electrothermal 8103 apparatus and are uncorrected. $^1$H NMR and $^{13}$C NMR spectra were recorded on Bruker 200 MHz or Varian 300 MHz spectrometer with TMS as internal standard. Splitting patterns are described as singlet (s), doublet (d), triplet (t), quartet (q), and broad (br); the value of chemical shifts ($\delta$) are given in ppm and coupling constants ($J$) in Hertz (Hz).

GC-MS were performed on a Saturn 3 (Varian) or Saturn 2000 (Varian) GC-MS System using a Chrompack DB5 capillary column (30 mm × 0.25 mm i.d.; 0.25 $\mu$m film thickness). FAB-MS spectra were performed using a VG 70-250S spectrometer. ESI-MS, APCI-MS spectra were performed by an Agilent 1100 series LC/MSD spectrometer and by LCQDeca-THERMOFINNIGAN spectrometer.

Elemental analyses were performed in a Perkin-Elmer 240C elemental analyzer, and the results were within ±0.4% of the theoretical values, unless otherwise noted.

Yields refer to purified products and are not optimized. All moisture-sensitive reactions were performed under argon atmosphere using oven-dried glassware and anhydrous solvents. All the organic layers were dried using anhydrous sodium sulfate.

1-(2,3-Dichlorophenyl)piperazine, 1-(3-methylphenyl)piperazine, and 1-(3-chlorophenyl)piperazine were commercially available, 1-(2,4-dichlorophenyl)piperazine was synthesized as previously described,[23] and 1-(3-cyanophenyl)piperazine was obtained starting from 3-cyanobromobenzene and piperazine following the same procedure described for the synthesis of 1-(2,4-dichlorophenyl)piperazine (spectroscopic data are consistent with those reported in the literature).[60]

For testing, compounds **5a**−**m** were transformed into the corresponding hydrochloride salts by a standard procedure.

**Ethyl 1-(Cyanomethyl)-7-methoxy-1*H*-indol-2-carboxylate (7).** A mixture of sodium hydride (60% dispersion in mineral oil, (849.2 mg, 21.23 mmol) and ethyl 7-methoxyindole-2-carboxylate **6** (3.1 g, 14.15 mmol) in dry DMF (15.0 mL) was stirred at room temperature for 30 min before the addition of bromoacetonitrile (2.0 mL, 28.3 mmol) in dry DMF (2.0 mL). The reaction mixture was then heated to 65 °C for 30 min and stirred for further 6 h at room temperature, and treated with ice. The separated solid was filtered and purified by means of flash chromatography (33% *n*-hexane in dichloromethane) to give **7** (30.1% yield) as a white solid: mp (ethanol) 99−101 °C. $^1$H NMR ($CDCl_3$) $\delta$ 1.41 (t, 3H, $J$ = 7.2 Hz), 3.99 (s, 3H), 4.40 (q, 2H, $J$ = 7.1 Hz), 5.96 (s, 2H), 6.80 (d, 1H, $J$ = 7.7 Hz), 7.10 (t, 1H, $J$ = 7.9 Hz), 7.25 (m, 1H), 7.33 (s, 1H). GC-MS $m/z$ 258 (100) $[M]^+$, 232, 213, 201, 187, 172, 144, 130, 114, 89.

**1,2,3,4-Tetrahydro-6-methoxypyrazino[1,2-*a*]indole (8).** A suspension of **7** (500.0 mg, 1.93 mmol) in dry diethyl ether ($Et_2O$) (20.0 mL) was added slowly to a well-stirred slurry of lithium aluminum hydride ($LiAlH_4$) (293.4 mg, 7.72 mmol) in dry $Et_2O$ (10.0 mL). The mixture was refluxed for 4 h and then poured into ice−water. 1 N NaOH (10.0 mL) was added and the aqueous phase

was extracted with EtOAc (3 × 30 mL). The collected organic layers were dried and evaporated. The crude product was chromatographed (10% methanol in chloroform) to afford **8** as a yellow solid (40.6% yield): mp (methanol) 120−122 °C. $^1$H NMR ($CDCl_3$) $\delta$ 1.89 (br s, 1H), 3.26 (t, 2H, $J$ = 5.7 Hz), 3.90 (s, 3H), 4.17 (s, 2H), 4.47 (t, 2H, $J$ = 5.8 Hz), 6.14 (s, 1H), 6.58 (d, 1H, $J$ = 7.7 Hz), 6.97 (t, 1H, $J$ = 7.7 Hz), 7.14 (d, 1H, $J$ = 7.8 Hz). ESI-MS $m/z$ 405 [2 M + H]$^+$, 203 (100) [M + H]$^+$.

**1,2,3,4-Tetrahydro-5-methoxy-*β*-carboline (13).** 4-Methoxytryptamine **12** (375.0 mg, 1.97 mmol) was transformed into the corresponding hydrochloride salt by a standard procedure. To a solution of 4-methoxytryptamine hydrochloride (445.0 mg, 1.97 mmol) in water (50.0 mL) glyoxylic acid monohydrate (181.2 mg, 1.97 mmol) was added and the mixture was stirred under reflux for 1 h. After cooling to room temperature, a 20% solution of NaOH was added and the mixture was extracted with EtOAc (3 × 30 mL). The organic layers were dried and evaporated. The crude product was chromatographed ($CHCl_3$/MeOH/$NH_4OH$ 20:5:0.5 v/v) to give **13** as an amorphous solid (63.2% yield). $^1$H NMR ($CDCl_3$) $\delta$ 1.67 (br s, 1H), 2.96 (m, 2H), 3.13 (m, 2H), 3.88 (s, 3H), 3.98 (s, 2H), 6.47 (d, 1H, $J$ = 7.6 Hz), 6.89 (d, 1H, $J$ = 8.1 Hz), 7.01 (t, 1H, $J$ = 7.9 Hz), 7.75 (br s, 1H).

**7-(4-Bromobutyloxy)quinoline (17a).** To a solution of 7-hydroxyquinoline **16a** (500.0 mg, 3.45 mmol) in dry DMF (15.0 mL), 1,4-dibromobutane (2.22 mL, 10.34 mmol) was added and the mixture was stirred at room temperature for 10 min. Then cesium carbonate (1.12 g, 3.45 mmol) was added and the mixture was heated to 65 °C for 12 h. After cooling to room temperature, methyl-*tert*-butylether (MTBE) (40.0 mL) and water (30.0 mL) were added and the mixture was extracted with MTBE (3 × 35 mL). The collected organic layers were dried, filtered, and evaporated. The residue was chromatographed (dichloromethane) to afford 645.0 mg of pure **17a** as a yellow oil (67.0% yield). $^1$H NMR ($CDCl_3$) $\delta$ 2.00 (m, 4H), 3.44 (t, 2H, $J$ = 5.9 Hz), 4.09 (t, 2H, $J$ = 5.1 Hz), 7.16 (m, 2H), 7.35 (d, 1H, $J$ = 2.5 Hz), 7.63 (d, 1H, $J$ = 8.9 Hz), 7.99 (m, 1H), 8.77 (m, 1H). ESI-MS $m/z$ 280, (100) [M + H]$^+$, 198.

**3-(4-Bromobutoxy)isoquinoline (17b).** Compound **17b** was obtained starting from isoquinolin-3-ol **16b** (250.0 mg, 1.72 mmol) and following the above-described procedure for **17a**. Compound **17b** was obtained as a yellow oil (52.0% yield). $^1$H NMR ($CDCl_3$) $\delta$ 2.07 (m, 4H), 3.50 (t, 2H, $J$ = 6.3 Hz), 4.38 (t, 2H, $J$ = 5.8 Hz), 6.36 (s, 1H), 7.35 (m, 1H), 7.55 (m, 1H), 7.67 (d, 1H, $J$ = 8.2 Hz), 7.86 (d, 1H, $J$ = 8.2 Hz), 8.92 (s, 1H). ESI-MS $m/z$ 302 [M + Na]$^+$, 280 [M + H]$^+$, 199 (100).

**3-(5-Bromopentyloxy)isoquinoline (17c).** Compound **17c** was obtained starting from isoquinolin-3-ol **16b** (200.0 mg, 1.37 mmol) and 1,5-dibromopentane following the above-described procedure for **17a**. Compound **17c** was obtained as a yellow oil (49.8% yield). $^1$H NMR ($CDCl_3$) $\delta$ 1.64 (m, 2H), 1.89 (m, 4H), 3.43 (t, 2H, $J$ = 6.5 Hz), 4.34 (t, 2H, $J$ = 6.3 Hz), 6.97 (s, 1H), 7.33 (m, 1H), 7.54 (t, 1H, $J$ = 7.2 Hz), 7.66 (d, 1H, $J$ = 8.3 Hz), 7.85 (d, 1H, $J$ = 8.2 Hz), 8.92 (s, 1H). ESI-MS $m/z$ 295 (100) [M + H]$^+$, 146.

***N*-[4-[4-(3-Cyanophenyl)piperazin-1-yl]butyl]benzo[*b*]furan-2-carboxamide (5a).** To a stirred solution of *N*-[4-(1-bromo)butyl]benzo[*b*]furan-2-carboxamide (**14a**) (50.0 mg, 0.17 mmol) in dry acetonitrile (3.0 mL), 1-(3-cyanophenyl)piperazine (31.7 mg, 0.17 mmol) and triethylamine (38.2 $\mu$L, 0.27 mmol) were added; the solution was refluxed for 12 h under stirring. The solvent was removed under reduced pressure, water was added, and the mixture was extracted with dichloromethane (3 × 10 mL). The organic layers were dried and concentrated and the crude product was chromatographed (10% MeOH in $CHCl_3$) to give 60.0 mg of **5a** (90.0% yield) as colorless oil. $^1$H NMR ($CDCl_3$) $\delta$ 1.72 (m, 4H), 2.46 (t, 2H, $J$ = 6.7 Hz), 2.61 (t, 4H, $J$ = 4.9 Hz), 3.24 (t, 4H, $J$ = 5.0 Hz), 3.52 (q, 2H, $J$ = 6.1 Hz), 6.89 (br s, 1H), 7.09 (m, 3H), 7.36 (m, 5H), 7.66 (d, 1H, $J$ = 7.5 Hz). FAB-MS $m/z$ 403 [M + H]$^+$, 147. Anal. ($C_{24}H_{26}N_4O_2$) C, H, N.

***N*-[4-[4-(2,3-Dichlorophenyl)piperazin-1-yl]butyl]isoquinoline-3-carboxamide (5b).** To a stirred solution of *N*-[1-(4-bromo)butyl]isoquinoline-3-carboxamide (**14b**) (100.0 mg, 0.33 mmol) in dry acetonitrile (10.0 mL), 1-(2,3-dichlorophenyl)piperazine hydrochloride (87.7 mg, 0.33 mmol) and triethylamine (74.0 $\mu$L, 0.53 mmol) were added and the solution was refluxed overnight under stirring. The solvent was removed under reduced pressure, water was added, and the mixture was extracted with dichlorometane (3 × 10 mL). The organic layers were dried and concentrated and the crude product was chromatographed (10% MeOH in $CHCl_3$) to give **5b** (60.2% yield) as a colorless oil. $^1$H NMR ($CDCl_3$) $\delta$ 1.67 (m, 4H), 2.47 (t, 2H, $J$ = 6.9 Hz), 2.64 (m, 4H), 3.06 (m, 4H), 3.57 (q, 2H, $J$ = 6.1 Hz), 6.92 (m, 1H), 7.11 (m, 2H), 7.70 (m, 2H), 7.98 (t, 2H, $J$ = 8.3 Hz), 8.33 (br s, 1H), 8.60 (s, 1H), 9.12 (s, 1H). $^{13}$C NMR ($CDCl_3$) $\delta$ 24.3, 27.6, 39.3, 51.3, 53.3, 58.0, 118.5, 120.1, 124.4, 127.3, 127.4, 127.5, 128.0, 128.7, 129.6, 130.9, 133.9, 136.0, 143.7, 150.9, 151.3, 164.7. ESI-MS $m/z$ 457 [M + H]$^+$, ESI-MS/MS of [M + H]$^+$ 285, 227 (100). Anal. ($C_{24}H_{26}Cl_2N_4O$) C, H, N.

***N*-[4-[4-(3-Chlorophenyl)piperazin-1-yl]butyl]isoquinoline-3-carboxamide (5c).** The title compound was prepared starting from **14b** (190.0 mg, 0.62 mmol) and 1-(3-chlorophenyl)piperazine hydrochloride (144.0 mg, 0.62 mmol) following the above-described procedure for **5b**. Compound **5c** was obtained as a white solid (50.4% yield): mp (methanol) 156−157 °C. $^1$H NMR ($CDCl_3$) $\delta$ 1.65 (m, 4H), 2.46 (t, 2H, $J$ = 6.7 Hz), 2.60 (t, 4H, $J$ = 4.9 Hz), 3.21 (t, 4H, $J$ = 5.0 Hz), 3.57 (q, 2H, $J$ = 6.5 Hz), 6.78 (m, 2H), 6.86 (d, 1H, $J$ = 1.6 Hz), 7.14 (t, 1H, $J$ = 8.0 Hz), 7.72 (m, 2H), 8.00 (t, 2H, $J$ = 8.2 Hz), 8.33 (br s, 1H), 8.61 (s, 1H), 9.14 (s, 1H). $^{13}$C NMR ($CDCl_3$) $\delta$ 24.6, 27.9, 39.5, 48.7, 53.1, 58.2, 114.0, 115.9, 119.4, 120.4, 127.8, 128.3, 128.9, 129.8, 130.2, 131.2, 135.1, 136.2, 144.0, 151.2, 152.5, 165.0. ESI-MS $m/z$ 445 (100) [M + Na]$^+$, 423 [M + H]$^+$, ESI-MS/MS of [M + H]$^+$ 251, 227 (100). Anal. ($C_{24}H_{27}ClN_4O$) C, H, N.

***N*-[4-(3,4-Dihydro-6-methoxypyrazino[1,2-*a*]1ndol-2(1*H*)-yl)-butyl]isoquinoline-3-carboxamide (5d).** To a suspension of 1,2,3,4-tetrahydro-6-methoxypyrazino[1,2-*a*]indole (**8**) (120.0 mg, 0.32 mmol) and $K_2CO_3$ (160.0 mg, 1.22 mmol) in dry acetonitrile (5.0 mL), bromo-derivative **14b** (98.0 mg, 0.32 mmol) and a catalytic amount of NaI were added and the resulting mixture was heated under reflux for 18 h. Thereafter the mixture was filtered and the filtrate was evaporated to dryness under reduced pressure. The residue was suspended in water (10.0 mL) and extracted with $Et_2O$ (2 × 25 mL) and dichloromethane (1 × 25 mL). The combined organic layers were evaporated under reduced pressure, and the crude product was purified by means of flash chromatography (0.5% MeOH in $CHCl_3$) affording to **5d** as a yellow oil (55.0% yield). $^1$H NMR ($CDCl_3$) $\delta$ 1.75 (m, 4H), 2.60 (m, 2H), 2.89 (t, 2H, $J$ = 5.5 Hz), 3.57 (q, 2H, $J$ = 6.1 Hz), 3.79 (s, 2H), 3.86 (s, 3H), 4.49 (t, 2H, $J$ = 5.6 Hz), 6.12 (s, 1H), 6.53 (d, 1H, $J$ = 7.6 Hz), 6.93 (t, 1H, $J$ = 7.7 Hz), 7.10 (d, 1H, $J$ = 7.9 Hz), 7.70 (m, 2H), 7.97 (m, 2H), 8.39 (br s, 1H), 8.59 (s, 1H), 9.05 (s, 1H). ESI-MS $m/z$ 879 [2 M + Na]$^+$, 451 [M + Na]$^+$, 429 (100) [M + H]$^+$. Anal. ($C_{26}H_{28}N_4O_2 \cdot {}^1/_2H_2O$) C, H, N.

***N*-[4-(1,2,3,4-Tetrahydro-5-methoxy-*β*-carbolin-2-yl)butyl]isoquinoline-3-carboxamide (5e).** The title compound was obtained following the procedure described for **5d**, starting from 1,2,3,4-tetrahydro-5-methoxy-$\beta$-carboline (**13**) (94.0 mg, 0.55 mmol) and **14b** (137.0 mg, 0.45 mmol). Compound **5e** was obtained as a yellow oil (30.0% yield). $^1$H NMR ($CDCl_3$) $\delta$ 1.74 (m, 4H), 2.64 (m, 2H), 2.82 (m, 2H), 3.03 (m, 2H), 3.57 (m, 4H), 3.86 (s, 3H), 6.44 (d, 1H, $J$ = 7.5 Hz), 6.92 (m, 2H), 7.72 (m, 2H), 7.97 (m, 3H), 8.39 (br s, 1H), 8.59 (s, 1H), 9.07 (s, 1H). ESI-MS $m/z$ 429 (100) [M + H]$^+$, 256, 227. Anal. ($C_{26}H_{28}N_4O_2$) C, H, N.

***N*-[4-[4-(3-Cyanophenyl)piperazin-1-yl]butyl]3,4-dihydropyrazino[1,2-*a*]indol-1(2*H*)-one (5f).** The title compound was prepared starting from **15** (190.0 mg, 0.59 mmol) and 1-(3-cyanophenyl)piperazine (110.3 mg, 0.59 mmol) following the same procedure described for compound **5a**. Compound **5f** was obtained as a colorless oil (60.0% yield). $^1$H NMR ($CD_3OD$) $\delta$ 1.83 (m, 4H), 3.24 (m, 6H), 3.70 (m, 4H), 3.92 (m, 4H), 4.37 (m, 2H), 7.13 (m, 2H), 7.23 (m, 1H), 7.33 (m, 3H), 7.44 (m, 2H), 7.66 (m, 1H). ESI-MS $m/z$ 428, (100) [M + H]$^+$, 241, 199. Anal. ($C_{26}H_{29}N_5O$) C, H, N.

***N*-[4-[4-(2,4-Dichlorophenyl)piperazin-1-yl]butyl]3,4-dihydropyrazino[1,2-*a*]indol-1(2*H*)-one (5g).** The title compound was prepared starting from bromoderivative **15** (200.0 mg, 0.63 mmol) and 1-(2,4-dichlorophenyl)piperazine (145.0 mg, 0.63 mmol) following the same procedure described for **5a**. Compound **5g** was obtained as a yellow oil (87.4% yield). $^1$H NMR ($CDCl_3$) $\delta$ 1.68 (m, 4H), 2.51 (m, 2H), 2.66 (m, 4H), 3.05 (m, 4H), 3.65 (t, 2H, $J$ = 7.1 Hz), 3.78 (t, 2H, $J$ = 5.7 Hz), 4.28 (m, 2H), 6.94 (d, 1H, $J$ = 8.4 Hz), 7.16 (m, 2H), 7.31 (m, 4H), 7.71 (d, 1H, $J$ = 7.8 Hz). ESI-MS $m/z$ 471, (100) $[M + H]^+$, 285, 241, 199. Anal. ($C_{25}H_{28}Cl_2N_4O \cdot {}^1/_2H_2O$) C, H, N.

***N*-[4-[4-(2,3-Dichlorophenyl)piperazin-1-yl]butyl]3,4-dihydropyrazino[1,2-*a*]indol-1(2*H*)-one (5h).** The title compound was prepared starting from **15** (270.0 mg, 0.84 mL) and 1-(2,3-dichlorophenyl)piperazine (193.0 mg, 0.84 mmol) following the same procedure described for **5a**. Compound **5h** was obtained as a white solid (78.2% yield): mp (methanol) 160−161 °C. $^1$H NMR ($CDCl_3$) $\delta$ 1.65 (m, 4H), 2.46 (t, 2H, $J$ = 7.2 Hz), 2.62 (m, 4H), 3.06 (m, 4H), 3.64 (t, 2H, $J$ = 6.5 Hz), 3.78 (t, 2H, $J$ = 6.0 Hz), 4.26 (t, 2H, $J$ = 5.3 Hz), 6.93 (m, 2H), 7.14 (m, 3H), 7.31 (m, 2H), 7.70 (d, 1H, $J$ = 8.0 Hz). ESI-MS $m/z$ 472 (100) $[M + H]^+$, 285, 241, 199, 172, 144. Anal. ($C_{25}H_{28}Cl_2N_4O$) C, H, N.

***N*-(4-(4-(*m*-Tolyl)piperazin-1-yl)butyl)benzo[*b*]furan-2-carboxamide (5i).** To a stirred solution of **14a** (620.0 mg, 2.09 mmol) in dry acetonitrile (30.0 mL) under argon, 1-(*m*-tolyl)piperazine dihydrochloride (443.0 mg, 2.09 mmol) and triethylamine (620 $\mu$L, 4.60 mmol) were added and the solution was refluxed overnight under stirring. The solvent was removed under reduced pressure, water was added, and the mixture was extracted with dichloromethane (3 × 30 mL). The organic layers were dried and concentrated, and the crude product was chromatographed (6% MeOH in $CHCl_3$) to give 0.42 g of **5i** (52.0% yield) as white solid: mp (methanol) 119−120 °C. $^1$H NMR ($CDCl_3$) $\delta$ 1.70 (m, 4H), 2.31 (s, 3H), 2.46 (t, 2H, $J$ = 6.6 Hz), 2.62 (t, 4H, $J$ = 4.9 Hz), 3.23 (t, 4H, $J$ = 4.9 Hz), 3.52 (q, 2H, $J$ = 6.1 Hz), 6.70 (m, 3H), 7.00 (br s, 1H), 7.13 (t, 1H, $J$ = 4.4 Hz), 7.33 (m, 4H), 7.66 (d, 1H, $J$ = 7.7 Hz). $^{13}$C NMR ($CDCl_3$) $\delta$ 22.0, 24.5, 27.7, 39.4, 49.3, 53.5, 58.1, 110.5, 111.9, 113.4, 117.1, 120.9, 122.9, 123.9, 127.0, 127.9, 129.2, 139.0, 149.2, 151.5, 154.9, 159.1. ESI-MS $m/z$ 805 (100) $[2 M + Na]^+$, 414 $[M + Na]^+$, 392 $[M + H]^+$. Anal. ($C_{24}H_{29}N_3O_2$) C, H, N.

**7-[4-[4-(2,3-Dichlorophenyl)piperazin-1-yl]butyloxy]quinoline (5j).** The title compound was prepared starting from **17a** (160.0 mg, 0.57 mmol) and 1-(2,3-dichlorophenyl)piperazine hydrochloride (153.4 mg, 0.57 mmol) following the procedure described for the synthesis of **5b**. Compound **5j** was obtained as a colorless oil (62.4% yield). $^1$H NMR ($CDCl_3$) $\delta$ 1.85 (m, 4H), 2.50 (t, 2H, $J$ = 7.4 Hz), 2.66 (m, 4H), 3.06 (t, 4H, $J$ = 4.3 Hz), 4.16 (t, 2H, $J$ = 6.0 Hz), 6.93 (m, 2H), 7.14 (m, 1H), 7.24 (m, 2H), 7.40 (d, 1H, $J$ = 2.3 Hz), 7.68 (d, 1H, $J$ = 8.9 Hz), 8.05 (d, 1H, $J$ = 8.0 Hz), 8.81 (m, 1H). ESI-MS $m/z$ 430 $[M + H]^+$. Anal. ($C_{23}H_{25}Cl_2N_3O$) C, H, N.

**3-[4-[4-(2,3-Dichlorophenyl)piperazin-1-yl]butoxy]isoquinoline (5k).** The title compound was prepared starting from **17b** (250.0 mg, 0.89 mmol) and 1-(2,3-dichlorophenyl)piperazine hydrochloride (237.0 mg, 0.89 mmol) following the procedure described for the synthesis of **5b**. Compound **5k** was obtained as a white amorphous solid (61.0% yield). $^1$H NMR ($CDCl_3$) $\delta$ 1.81 (m, 4H), 2.52 (t, 2H, $J$ = 7.3 Hz), 2.66 (m, 4H), 3.06 (m, 4H), 4.38 (t, 2H, $J$ = 6.3 Hz), 6.94 (m, 2H), 7.13 (m, 2H), 7.36 (m, 1H), 7.56 (t, 1H, $J$ = 7.3 Hz), 7.67 (d, 1H, $J$ = 8.2 Hz), 7.87 (d, 1H, $J$ = 8.1 Hz), 8.94 (s, 1H). ESI-MS $m/z$ 452 $[M + Na]^+$, 430 (100) $[M + H]^+$. Anal. ($C_{23}H_{25}Cl_2N_3O$) C, H, N.

**3-[5-[4-(2,3-Dichlorophenyl)piperazin-1-yl]pentyloxy]isoquinoline (5l).** The title compound was prepared starting from **17c** (325.0 mg, 1.11 mmol) and 1-(2,3-dichlorophenyl)piperazine hydrochloride (295.0 mg, 1.11 mmol) following the procedure described for synthesis of **5b**. Compound **5l** was obtained as a white amorphous solid (54.3% yield), mp (methanol) 133−134 °C. $^1$H NMR ($CDCl_3$) $\delta$ 1.53 (m, 4H), 1.86 (m, 2H), 2.42 (m, 2H), 2.61 (m, 4H), 3.03 (m, 4H), 4.32 (m, 2H), 6.92 (m, 2H), 7.10 (m, 2H), 7.32 (t, 1H, $J$ = 7.4 Hz), 7.52 (t, 1H, $J$ = 7.5 Hz), 7.64 (d, 1H, $J$ = 8.4 Hz), 7.83 (d, 1H, $J$ = 8.2 Hz), 8.91 (s, 1H). ESI-MS $m/z$ 466 $[M + Na]^+$, 444 (100) $[M + H]^+$, 299. Anal. ($C_{24}H_{27}Cl_2N_3O$) C, H, N.

**3,4-Dihydro-2-[4-(3,4-dihydro-6-methoxypyrazino[1,2-*a*]indol-2(1*H*)-yl)butyl]pyrazino[1,2-*a*]indol-1(2*H*)-one (5m).** The title compound was prepared starting from bromo-derivative **15** (47.7 mg, 0.15 mmol) and 1,2,3,4-tetrahydro-6-methoxypyrazino[1,2-*a*]indole **8** (30.0 mg, 0.15 mmol) following the procedure described for the synthesis of compound **5d**. Compound **5m** was obtained as a yellow oil (62.0% yield). $^1$H NMR ($CDCl_3$) $\delta$ 1.69 (m, 4H), 2.58 (t, 2H, $J$ = 6.6 Hz), 2.88 (t, 2H, $J$ = 5.5 Hz), 3.66 (t, 2H, $J$ = 6.7 Hz), 3.77 (m, 4H), 3.88 (s, 3H), 4.24 (t, 2H, $J$ = 5.8 Hz), 4.45 (t, 2H, $J$ = 5.6 Hz), 6.10 (s, 1H), 6.54 (d, 1H, $J$ = 7.6 Hz), 6.93 (t, 1H, $J$ = 7.8 Hz), 7.13 (m, 3H), 7.29 (m, 2H), 7.70 (d, 1H, $J$ = 7.9 Hz). $^{13}$C NMR ($CDCl_3$) $\delta$ 24.3, 25.3, 29.6, 40.2, 45.5, 45.9, 46.1, 51.2, 51.7, 55.3, 57.2, 97.1, 101.8, 106.0, 109.5, 112.9, 120.6, 122.6, 124.3, 125.9, 127.5, 129.4, 130.3, 134.5, 136.3, 147.7, 159.9. ESI-MS $m/z$ 907 $[2 M + Na]^+$, 884 $[2 M + H]^+$, 443 (100) $[M + H]^+$. Anal. ($C_{27}H_{30}N_4O_2 \cdot {}^1/_3H_2O$) C, H, N.

**Molecular Modeling.** Molecular modeling calculations were performed on SGI Origin 200 8XR12000, while molecular modeling graphics were carried out on SGI Octane 2 and Octane workstations.

**Homology Modeling.** Originally we choose the bovine rhodopsin's crystal structures in the inactivated and partially activated states downloaded from the PDB data bank (http://www.rcsb.org/pdb/; PDB IDs: 1U19 and 2I37, respectively) as templates for the modeling of the 7TMs region of human $D_2R$ and $D_3R$ and human $5HT_{1A}R$, $5HT_{2A}R$, and $5HT_{2C}R$. Subsequently, after the publication of the X-ray structures of the human $\beta_2$-adrenergic receptor, we also used this receptor as template, choosing the structure with the higher resolution[38] (PDB ID: 2RH1, $R$ = 2.4 Å) for the modeling of dopaminergic and serotoninergic receptors TMs in the partially inactivated state. Hereafter, we will refer to a common computational procedure applied for the generation of all receptor models in each activation state.

To be sure of correctly predicting the "7TMs" region of our receptor models, we first performed a secondary structure prediction test on the template sequences (i.e., bovine rhodopsin and $\beta_2$-adrenergic receptors) by using the Structure Prediction and Sequence Analysis (PredictProtein) server (http://www.predictprotein.org/). The correctness of the prediction was then verified against the X-ray structures. On the basis of the results obtained, $D_2R$, $D_3R$, $5\text{-}HT_{1A}R$, $5\text{-}HT_{2A}R$, and $5\text{-}HT_{2C}R$ sequences were subjected to the same PredictProtein server (http://www.predictprotein.org/) calculation. Accordingly, we modeled the 7TMs regions of the dopamine and serotonin receptors by aligning the following sequence portions of the templates (PDB numbering). Bovine rhodopsin: TM1 = 33−66, TM2 = 70−100, TM3 = 106−141, TM4 = 151−173, TM5 = 199−230, TM6 = 244−278, TM7 = 285−310; human $\beta_2$-adrenergic receptor: TM1 = 29−62, TM2 = 66−96, TM3 = 102−137, TM4 = 148−170, TM5 = 195−225, TM6 = 265−299, TM7 = 305−330, with the dopamine/serotonin receptors segments predicted to assume an α-helix secondary structure and to have a transmembranarian location.

Second, to be sure of properly aligning the sequences of the templates and of the receptors to be modeled, we performed an alignment test on the template sequences by using either Bioinfo (http://cheminfo.u-strasbg.fr) or ClustalW (http://www.ebi.ac.uk/Tools/clustalw2/).

The ligands, 11-*cis*-retinal (1U19) and carazolol (2RH1), were removed using the *Unmerge* command in the Biopolymer module of Insight2005 (Accelrys, San Diego). A.car and an.mdf file were generated for the coordinates of the 7TMs region of each template. Template sequences were extracted from the 3D structures by using the *Extract* command in the *Sequence* pulldown of the Homology module (Insight2005) and manually aligned to that of each receptor subtype, taking into account the results obtained from: (a) PredictProtein (http://www.predictprotein.org/) analysis, (b) ConSeq (http://conseq.bioinfo.tau.ac.il/) analysis, (c) ClustalW (http://www.ebi.ac.uk/Tools/clustalw2/) multiple alignment, (d) Bioinfo (http://cheminfo.u-strasbg.fr) multiple alignment, (e) mutagenesis studies,[35] and (f)

Eukaryotic Linear Motif server sequence analysis (http://elm.eu.org/) and protein structural domains analysis,[61] aimed at identifying linear functional motifs and structural domains possibly involved in protein−protein interactions. The resulting multiple sequence alignment is reported in the Supporting Information.

The coordinates of the 7TMs for each model were assigned as follows. Boxes were created and frozen around each sequence segment of the model aligned with the corresponding TM of the template protein (Homology module; Insight2005). These sequence segments represented the putative 7TMs of the receptor models and were defined as structural conserved regions (SCR). Coordinates were assigned using the *SCR-AssignCoords* command of the *Sequence* pulldown. In particular, for template/model identical side chains, the coordinates for the whole amino acid were transferred. However, when the side chain of the model differed from that of the template, backbone coordinates were transferred while side chain atoms coordinates were assigned by aligning the side chain dihedral angles with the corresponding template residue. This was to preserve the conformation of the reference side chain as much as possible. Eventual bumps were removed by manually changing the torsion angles or by means of the *Manual_Rotamer* command of the *Residue* pulldown of the Homology module. Hydrogens were added to all amino acids considering a pH value of 7.2. The C- and N-terminus of each helix were capped with an aldheydic and an $N_{sp2}H_2$ group, respectively, to avoid unrealistic ionic contacts.

The receptor model optimization procedure was carried out by using the Discover3 module of Insight2005. Every structure was progressively relaxed (Cell Multipole summation method for nonbond interactions,[62] $\varepsilon = 4r$, CVFF force field).[63] First, an initial optimization of side chain interactions was performed, keeping the backbone atoms fixed (algorithms: Steepest Descent until the maximum rms derivative was less than 0.5 kcal/Å, Conjugate Gradient from a derivative of 0.5 to less than 0.1 kcal/Å). Subsequently, the backbone was relaxed through six minimization cycles by using the above-reported combination of Steepest Descent and Conjugate Gradient algorithms and applying different tether force values for each minimization cycle: from an initial value of 5 kcal/Å$^2$ to a final value of 0.1 kcal/Å$^2$. A final energy minimization round was performed with a residual tether force of 0.1 Kcal/ Å$^2$ applied only to backbone Cα atoms. Each energy minimization cycle was followed by a structural check by using the *Struct_Check* command of the *ProStat* pulldown in the Homology module to verify the correctness of the geometry optimization procedure before moving to the next minimization cycle. Checks included $\varphi$, $\Psi$, $\chi_1$, $\chi_2$, $\chi_3$, and $\omega$ dihedral angles, Cα virtual torsions, and Kabsch and Sander main chain H-bond energy evaluation. A full unconstrained geometry optimization has been attempted but produced unrealistic results considering that the system upon study is lacking in structural elements (i.e., loops, lipid bilayer, water molecules, etc.).

**Conformational Analysis for Compounds 5a−m.** Compounds **5a−m** were built using the Insight2005 Builder module. The apparent p$K_a$ values were estimated using the ACD/p$K_a$ DB version 11.00 software (Advanced Chemistry Development Inc., Toronto, Canada). According to the resulting values (Table 2 of the Supporting Information), in all subsequent calculations, all compounds were considered protonated at pH = 7.2 (cytoplasmic value) on the aliphatic nitrogen of the piperazine ring. Partial charges were assigned by using the CFF91 force field.[64]

The conformational space of compounds **5a−m** was sampled through 200 cycles of simulated annealing. An initial temperature of 1000 K was applied to the system for 1000 fs with the aim of surmounting torsional barriers. Successively, temperature was linearly reduced to 200 K with a decrement of 0.5 K/fs. The resulting structures were subjected to two protocols of energy minimization within Insight2005 Discover module (CFF91 force field, Conjugate Gradient algorithm; maximum rms derivative < 0.001 kcal/Å), which differed in the dielectric constant value, i.e. $\varepsilon = 80r$ and $\varepsilon = 1$, in order to maximize inter- or intramolecular interactions, respectively. All the resulting conformers were subsequently ranked in different families taking into account their conformational energy as well as some geometric parameters, such as: (a) the distance between the centroid of the phenyl ring at the tail and the centroid of the heteroaromatic ring at the head, (b) the orientation of the piperazine nitrogen hydrogen with respect to the position of the aromatic rings, (c) the conformation of the piperazine ring (i.e., *chair*, *half-chair*, and *boat*), (d) the dihedral angle value between the heteroatom of the heteroaryl moiety and the heteroatom X (amid or ether oxygen) of the linker, (e) the rotation of the phenyl ring with respect to the piperazine ring (i.e., dihedral angle value), and (f) the configuration of the amide group (i.e., cis or trans).

To properly analyze the electronic properties of the compounds, the most stable conformer of each family, within the range of 5 kcal/mol from the global minimum conformer ($\Delta E_{GM}$ < 5 kcal/mol), was subjected to a full geometry optimization through semiempirical calculations, using the quantum mechanical method AM1 in the Mopac2007 package.[65] The EF (eigenvector Following routine) algorithm of geometry optimization was used, with a GNORM value set to 0.01. The max step size parameter was set to 0.05 to tackle the convergence problems and to properly reach a full geometry optimization. With the same aim, the criteria for terminating all optimizations was increased by a factor of 100 using the keyword PRECISE. All the resulting conformers were subsequently ranked in different families using the same energy and geometry criteria reported above.

The dipole moments were calculated using partial charges obtained by the quantum mechanical method AM1 (Mopac2007) and visualized as vector by using the Decipher module of Insight2005.

**Pharmacology.** Procedures involving animals and their care were conducted in conformity with the institutional guidelines that are in compliance with national (D.L. n. 116, G.U. suppl. 40, 18 Febbraio 1992, Circolare no. 8, G.U. Fourteen Luglio 1994) and international laws and policies (EEC Council Directives 86/609, OJL 358, 1, Dec. 12, 1987; Guide for the Care and Use of laboratory Animals, U.S. National Research Council, 1996).

**1. In Vitro Binding Assays on GPCRs.**[22a,b,23] **Serotonin and Dopamine Receptors.** Male CRL:CD(SD)BR-COBS rats and male CRL:(HA) BR albino guinea pig (Charles River, Italy) were killed by decapitation; their brains were rapidly dissected into the various areas (rat striatum for $D_1$R and $D_2$R, rat hippocampus for 5-$HT_{1A}$R, rat cortex for 5-$HT_{2A}$R and guinea pig cortex for 5-$HT_{2C}$R) and stored at − 80 °C until assay. Binding was calculated on rat tissue homogenates ($D_1$, $D_2$, 5-$HT_{2A}$, and 5-$HT_{2C}$ receptors) and on Sf9 cell membranes ($D_{3r}$). Tissues were homogenized in about 50 volumes of ice-cold Tris HCl, 50 mM, pH 7.4 (for $D_1$R, $D_2$R, and 5-$HT_{2A}$R) using an Ultra-Turrax TP-1810 homogenizer (2 × 20 s) and centrifuged at 50000*g* for 10 min at 4 °C (Beckman J-25 centrifuge). Each pellet was resuspended in the same volume of fresh buffer, incubated at 37 °C for 10 min, and centrifuged again at 50000*g* for 10 min at 4 °C. The pellet was then washed once by resuspension in fresh buffer and centrifuged as before. The resulting pellets were resuspended just before the binding assay in the appropriate incubation buffer 50 mM Tris HCl, pH 7.4, containing 10 μM pargyline, 0.1% ascorbic acid, 120 mM NaCl, 5 mM KCl, 2 mM $CaCl_2$, 1 mM $MgCl_2$ for $D_1$R and $D_2$R; 50 mM Tris HCl, pH 7.4, containing 10 μM pargyline and 4 mM $CaCl_2$ for 5-$HT_{1A}$R; 50 mM Tris HCl, pH 7.7 for 5-$HT_{2A}$R; 50 mM Tris HCl, pH 7.4, containing 10 μM pargyline, 4 mM $CaCl_2$; and 0.1% ascorbic acid for 5-$HT_{2C}$R). For $D_{3r}$ receptors, Sf9 cells membranes expressing $D_{3r}$ dopamine receptors (Signal Screen) were resuspended just before the binding assay in 50 mM Tris HCl, pH 7.4, containing 5 mM EDTA, 5 mM $MgCl_2$, 5 mM KCl, 1.5 mM $CaCl_2$, 120 mM NaCl.

[$^3$H]-SCH 23390 (specific activity, 75.5 Ci/mmol; NEN) binding to $D_1$R was assayed in a final incubation volume of 0.5 mL, consisting of 0.25 mL of membrane suspension (striatum 2.5 mg of tissue/sample), 0.25 mL of [$^3$H]ligand (0.4 nM) and 10 μL of displacing agent or solvent. Nonspecific binding was obtained in the presence of 10 μM (−)*cis*-flupentixol.

[$^3$H]-Spiperone (specific activity, 25 Ci/mmol; NEN) binding to $D_2$R was assayed in a final incubation volume of 1 mL, consisting

of 0.5 mL of membrane suspension (striatum 2.5 mg of tissue/sample), 0.5 mL of [$^3$H]ligand (0.2 nM), and 20 $\mu$L of displacing agent or solvent. Nonspecific binding was obtained in the presence of 100 $\mu$M (−)sulpiride.

[$^3$H]-7-OH-DPAT (specific activity, 159 Ci/mmol; Amersham) binding to $D_{3r}$ receptors was assayed in a final incubation volume of 1 mL, consisting of 0.5 mL of membrane suspension (12 $\mu$g protein/sample), 0.5 mL of [$^3$H]ligand (0.7 nM), and 20 $\mu$L of displacing agent or solvent. Nonspecific binding was obtained in the presence of 1 $\mu$M dopamine.

[$^3$H]-8-OH-DPAT (specific activity, 217 Ci/mmol; Amersham) binding to 5-$HT_{1A}$R was assayed in a final incubation volume of 0.5 mL, consisting of 0.25 mL of membrane suspension (5 mg tissue/sample), 0.25 mL of [$^3$H]ligand (1 nM), and 10 $\mu$L of displacing agent or solvent. Nonspecific binding was obtained in the presence of 10 $\mu$M serotonin.

[$^3$H]-Ketanserin (specific activity, 88 Ci/mmol; Amersham) binding to 5-$HT_2$R was assayed in a final incubation volume of 1 mL, consisting of 0.5 mL of membrane suspension (5 mg of tissue/sample), 0.5 mL of [$^3$H]ligand (0.7 nM), and 20 $\mu$L of displacing agent or solvent. Nonspecific binding was obtained in the presence of 1 $\mu$M methisergide.

[$^3$H]-Mesulergine (specific activity, 90 Ci/mmol; Amersham) binding to 5-$HT_{2c}$R was assayed in a final incubation volume of 1 mL, consisting of 0.5 mL of membrane suspension (30 mg of tissue/sample), 0.5 mL of [$^3$H]ligand (1 nM), and 20 $\mu$L of displacing agent or solvent. Nonspecific binding was obtained in the presence of 10 $\mu$M mesulergine.

Incubations (15 min at 25 °C for $D_1$R, 15 min at 37 °C for $D_2$R and 5-$HT_{2A}$R, 30 min at 25 °C for 5-$HT_{1A}$R, 60 min at 25 °C for $D_{3r}$ receptors, 30 min at 37 °C for 5-$HT_{2C}$R) were stopped by rapid filtration under vacuum through GF/B (for $D_1$R, $D_2$R, 5-$HT_{1A}$R, 5-$HT_{2A}$R, and 5-$HT_{2C}$R) or GF/B presoaked with 0.3% polyethyleneimine for $D_3$R filters which were then washed with 12 mL (4 mL × 3 times) of ice-cold buffer (50 mM Tris HCl, pH 7.4) using a Brandel M-48R cell harvester. The radioactivity trapped on the filters was counted in 4 mL of Ultima Gold MV (Packard) in a $\beta$ counter (Wallac) with a counting efficiency of 50%. For all binding assays the radioactivity trapped on the filters was counted in 4 mL of Ultima Gold MV (Packard) in a LKB 1214 rack beta liquid scintillation spectrometer with a counting efficiency of 50%.

**Histamine $H_1$ Receptor.** Histamine $H_1$ receptor. Binding affinity was tested according to the procedure of Dini et al.[66] Binding was determined using membranes prepared from guinea pig cerebellum with [$^3$H]pyrilamine (0.5 nM) as radioligand.

**Adrenergic $\alpha_1$ Receptors.** Binding was determined using membranes prepared from rat cerebral cortex homogenized in phosphate buffer. The homogenate was centrifuged at 44000*g* for 10 min, and the pellet was suspended in phosphate buffer and washed two times more; 500 $\mu$L of this homogenate was incubated with 500 $\mu$L of 0.2 nM [$^3$H]prazosin and 20 $\mu$L of test compound for 30 min at 25 °C and then filtered through a Whatman GF/B filter (Whatman International Ltd.). Radioactivity on the filter was measured with a liquid scintillation counter. Complete (100%) inhibition of [$^3$H]prazosin binding was determined in the presence of 10 $\mu$M prazosin. Nonspecific binding was determined in the presence of 10 $\mu$M prazosin.

**Adrenergic $\alpha_2$ Receptors.** Binding was determined using membranes prepared from rat cerebral cortex homogenized in phosphate buffer. The homogenate was centrifuged at 44000*g* for 10 min, and the pellet was suspended in phosphate buffer and washed two times more; 500 $\mu$L of this homogenate was incubated with 500 $\mu$L of 1 nM [$^3$H]clonidine and 20 $\mu$L of test compound for 30 min at 25 °C and then filtered through a Whatman GF/B filter (Whatman International Ltd.). Nonspecific binding was determined in the presence of 10 $\mu$M clonidine.

**Imidazole $I_2$ Receptors.** Rabbit kidney was homogenized in 10 volumes of Tris-HCl buffer (50 mM, pH 7.4) and 250 mM sucrose and centrifuged at 500*g* for 10 min. The supernatant was centrifuged at 28000*g* for 30 min, and the resulting pellet was washed twice with the same buffer without sucrose. The final pellet was resuspended in Tris-HCl buffer (50 mM, pH 7.4) and stored at −80 °C until use. Rabbit kidney membranes (200 $\mu$g of protein) were incubated with 5 nM [$^3$H]idazoxan (Amersham, 43 Ci/mmol) in the absence or presence of a range of 10−12 concentrations of competing ligand drug in a total volume of 400 $\mu$L of assay buffer. To mask adrenoreceptors, 10 $\mu$M (−)-norepinephrine (in the presence of 0.005% ascorbic acid) was added to all tubes. Nonspecific binding was determined with 10 $\mu$M of cirazoline. Specific binding represented about 90% of the total binding at 5 nM [$^3$H]-idazoxan. Following equilibrium (45 min at 25 C), bound radioactivity was separated from free by filtration as described above. Each point was performed in triplicate.

Dose−inhibition curves were analyzed by the Allfit[67] program to obtain the concentration of unlabeled drug that caused 50% inhibition of ligand binding. The $K_i$ values were derived from the $IC_{50}$ values according to the method of Cheng and Prusoff.[68]

**2. In Vitro Assays for hERGAffinity Evaluation. Plasmids.** The human ERG and KCNE1 (potassium voltage-gated channel, Isk-related family, member 1) were subcloned into the mammalian expression vectors pNS1n and pNS1z, respectively, to produce the plasmid constructs pNS1n_hERG and pNS1Z-minK.

HEK 293 cells stably expressing hERG + KCNQ1 (potassium voltage-gated channel, KQT-like subfamily, member 1). HEK 293 tissue culture cells were transfected with equal amounts of the plasmids pNS1n_hERG and pNS1Z-minK using lipofection (Lipofectamin, Life Technologies). Expression of functional hERG channels was verified by patch-clamp measurements.

**Whole-Cell Recordings.** Cells plated on coverslips were placed in a 15 $\mu$L perfusion chamber (flowrate ∼1 mL/min = full exchange every 1 s). All experiments were performed at room temperature (20−22 °C) using EPC-9 patch-clamp amplifiers (HEKA-electronics, Lambrect, Germany). Series resistances as well as capacitance compensation were updated before each stimulus. Usually the cell capacitance ranged from 5 to 20 pF and the series resistances were in the range 3−6 MΩ.

**Fitting Procedure.** We assumed that the drugs (D) interacted with the receptors (R) in the following way:

$$R + D \underset{k_{off}}{\overset{k_{on}}{\leftrightarrow}} RD$$

This is a simple bimolecular reaction, which integrated under nonequilibrium conditions are described by equation 1:

$$I_t = I_0(1 - (C/C + K_i * (1 - \exp^{-t(C*k_{on}+k_{off})}))) \quad (1)$$

Where $I_t$ = current at time 1 in nA, $I_0$ = unblocked current in nA, $C$ = drug concentration in M, $k_{off}$ = off-rate in $s^{-1}$, $k_{on}$ = on-rate in $M^{-1}s^{-1}$, $K_i = k_{off}/k_{on}$. At $t = \infty$ eq 1 simplifies to Michaelis−Menten equation with $K_i = IC_{50}$.

The peak tail-current was plotted versus time. The blocker-induced decrease in current versus time was fitted to eq (1) to give $k_{on}*k_{off}$ and thereby $k_i$. Each value is the mean ± SD of 2−8 determinations and represents $\mu$M values.

**3. Experimental in Vitro Pharmacology for Intrinsic Activity Assessment. 3.1. Cell-Based Assays. Dopamine $D_{2L}$ Receptors.** For evaluation of [$^{35}$S]-GTP$\gamma$S binding to $D_{2L}$ receptors, human CHO cells Chinese hamster ovary in DMSO (0.4%) vehicle were resuspended in Hepes 20 mM, pH 7.4, containing 100 mM NaCl, 1 mM EDTA, 10 mM $MgCl_2$, 1 mM DTT, in a glass/Teflon potter. The binding assay was carried out in a final incubation volume of 120 $\mu$L, consisting of 100 $\mu$L of membrane suspension (about 15 $\mu$g of protein/sample), 10 $\mu$L of [$^{35}$S]-GTP$\gamma$S (final concentration 1 nM), and 10 $\mu$L of displacing agent or solvent. Nonspecific binding was obtained in the presence of 10 $\mu$M GTP$\gamma$S; samples were preincubated for 15 min at 30 °C without [$^{35}$S]-GTP$\gamma$S and then for 15 min at 30 °C with [$^{35}$S]-GTP$\gamma$S.

**Dopamine $D_{2S}$ Receptors.** For evaluation of [$^{35}$S]-GTP$\gamma$S binding to $D_{2S}$ receptors, human CHO cells Chinese hamster ovary in DMSO (1%) vehicle were resuspended in Hepes 20 mM, pH 7.4, containing 100 mM NaCl, 1 mM EDTA, 10 mM $MgCl_2$, 1 mM DTT, in a glass/Teflon potter. The binding assay was carried

out in a final incubation volume of 120 $\mu$L, consisting of 100 $\mu$L of membrane suspension (about 15 $\mu$g of protein/sample), 10 $\mu$L of [$^{35}$S]- GTP$\gamma$S (final concentration 1 nM), and 10 $\mu$L of displacing agent or solvent.

Nonspecific binding was obtained in the presence of 10 $\mu$M GTP$\gamma$S; samples were preincubated for 15 min at 30 °C without [$^{35}$S]-GTP$\gamma$S and then for 30 min at 30 °C with [$^{35}$S]-GTP$\gamma$S.

**Dopamine $D_3$ Receptors.** For evaluation of [$^{35}$S]-GTP$\gamma$S binding to $D_3$ receptors, human CHO-K1 cells Chinese hamster ovary in DMSO (1%) vehicle were resuspended in Hepes 20 mM, pH 7.4, containing 100 mM NaCl, 1 mM EDTA, 10 mM $MgCl_2$, 1 mM DTT, in a glass/Teflon potter. The binding assay was carried out in a final incubation volume of 120 $\mu$L, consisting of 100 $\mu$L of membrane suspension (about 15 $\mu$g of protein/sample), 10 $\mu$L of [$^{35}$S]- GTP$\gamma$S (final concentration 1 nM), and 10 $\mu$L of displacing agent or solvent.

Nonspecific binding was obtained in the presence of 10 $\mu$M GTP$\gamma$S; samples were preincubated for 15 min at 30 °C without [$^{35}$S]-GTP$\gamma$S and then for 30 min at 30 °C with [$^{35}$S]-GTP$\gamma$S.

**3.2. Tissue Assays. Serotonin 5-$HT_{1A}$ Receptors.** For 5-$HT_{1A}$R intrinsic activity assessment, Duncan Hartley guinea pig ileum 325 ± 25 g were taken in DMSO (0.1%) vehicle and were put in the incubation buffer (Krebs, pH 7.4) and were incubated 5 min at 32 °C. The final volume of the bath was brought to 10 mL. After 5 min, the quantitation method was isometric (gram changes). Significant criteria: agonism ≥50% reduction of neurogenic twitch relative to 0.12 $\mu$M 8-OHDPAT response. Significant criteria: antagonism ≥50% inhibition of 0.12 $\mu$M 8-OHDPAT-induced relaxation.

**Serotonin 5-$HT_{2A}$ Receptors.** For 5-$HT_{2A}$R intrinsic activity assessment, Wistar rat 275 ± 25 g aortic ring was taken in DMSO (0.1%) vehicle and was put in the incubation buffer (Krebs at pH 7.4) and was incubated 5 min at 37 °C. The final volume of the bath was brought to 10 mL. After 5 min, the quantitation method was isometric (gram changes). Significant criteria: agonism ≥50% contraction response relative to 3 $\mu$M 5-HT response. Significant criteria: antagonism ≥50% inhibition of 3 $\mu$M 5-HT induced contraction.

**4. Behavioral Tests.** All experimental procedures carried out in this study were in compliance with the European Communities Council Directive of 24 November 1986 (86/609/EEC) and approved by the Danish Animal Welfare Committee, appointed by the Danish Ministry of Justice.

Male Wistar rats (200−225 gr) or female NMRI mice (Taconic M&B, P.O. Box 1079, DK-8680 Ry, Denmark) kept in a ventilated closed rack (Scantainer, Scanbur Ltd., Denmark) at constant temperature (21 °C) and humidity (60−70%) with a 7:00 a.m. light/7:00 p.m dark cycle were used in these studies. Food (Altromin rat pellets) and water were available ad libitum. Experiments were conducted during daytime in the light phase. The animals were habituated to the experimental room approximately 24 h before start of the experiments.

**5c, 5h, 5i, 5l.** Aripiprazole (Sequoia Research Products Ltd.), and Clozapine (RBI) were dissolved in 10% Tween 80 and diluted to final concentration by adding appropriate volume of 0.9% NaCl. Haloperidol (Seranase, Janssen-Cilag, ampules of 5 mg/mL), S-(+)-Methamphetamine-HCl (RBI) and Phencyclidine (PCP, synthesized at NeuroSearch A/S) were dissolved in 0.9% NaCl. All test- and reference compounds were administered subcutaneously (sc) 30 min before test start in a dose volume of 10 mL/kg. MAMP and PCP were dosed intraperitoneally (ip) and sc, respectively, and administered in a dose volume of 10 mL/kg immediately before test start. Appropriate doses of **5c**, **5h**, **5i**, and **5l** were chosen based on initial behavioral observations.

**Exploratory Locomotor Activity.** Exploratory locomotor activity was assessed in 14 automated activity frames (TSE Home Cage Activity Monitoring System, MoTil, TSE Technical and Scientific Equipment GmbH, Germany) equipped with infrared photobeam emitters and sensors. To assess drug effect on exploratory locomotor activity, the mice were transferred to new home cages immediately before test start and activity was measured for 30 min. Test or reference compounds were administered 30 min before test start at the following doses: **5c**, **5h**, and **5l**: 3, 10, 30 mg/kg; **5i**: 1, 3, 10 mg/kg; aripiprazole: 0.1, 0.3, 1.0, 3.0 mg/kg; clozapine: 0.3, 1, 3 mg/kg; haloperidol: 0.025, 0.05, 0.1, 0.2 mg/kg.

**MAMP- and PCP-Induced Hyperactivity.** MAMP- and PCP-induced hyperactivity was measured in automated activity frames as described above. MAMP and PCP were administered in a dose of 2 and 4 mg/kg, respectively. Both compounds were dosed immediately before test start. In the MAMP study, test or reference compounds were pretreated 30 min before test start at the following doses: **5h**, **5c**, **5i**, and **5l**: 1, 3, and 10 mg/kg; aripiprazole: 0.1, 0.3, and 1.0 mg/kg; clozapine: 0.3, 1, and 3 mg/kg; haloperidol: 0.025, 0.05, and 0.1 mg/kg. Locomotor activity was measured for a total of 120 min. In the PCP study, test or reference compounds were administered 30 min before test start at the following doses: **5h**: 0.3, 1, 3 mg/kg; **5c**, **5i**, and **5l**: 1, 3, and 10 mg/kg; aripiprazole: 0.1, 0.3, and 1.0 mg/kg; clozapine: 0.3, 1.0, and 3.0 mg/kg; haloperidol: 0.01, 0.025, and 0.05 mg/kg. Locomotor activity was measured for 60 min.

**Catalepsy.** Cataleptogenic potential of the compounds was assessed in the horizontal bar test consisting of a horizontal bar with a diameter of 2 mm and elevated 4 cm above ground. Test or reference compound was administered sc 30 min before the first catalepsy assessment. Hereafter, the degree of catalepsy was scored every 15 min for a total of 45 min.

**Statistics.** Drug effects on exploratory and stimulant-induced locomotor activity were analyzed by applying a two-way ANOVA with drug effect and time interval as factors. Drug-induced catalepsy was evaluated by one-way ANOVA with treatment as factor. $P$ values $< 0.05$ were considered statistically significant.

**5. Fos Induction After Acute Administration of 5i.** Rats ($n$ = 5 pr group) were injected i.p. with a single dose of **5i** (3, 10, 15, or 30 mg/kg) or vehicle (5% Chremophor) and returned to their home-cage. One hour after drug administration, the rat was deeply anaesthetized with mebumal (50 mg/mL, 3 mL/kg) and perfused transcardially with 0.1 M phosphate buffered saline (PBS; pH = 7.4) followed by fixation in 4% paraformaldehyde-PBS for 10 min.[69] Then 40 $\mu$m serial coronal sections were cut through the forebrain in series of four and processed for c-Fos immunoreactivity according to earlier report.[69] Prior to the immunocytochemical steps, the sections were rinsed for 3 × 10 min in 0.01 M PBS, incubated for 10 min in 1% $H_2O_2$−PBS to block endogenous peroxidase activity, and for a minimum of 20 min in 0.01 M PBS with 0.3% Triton X-100 (TX), 5% swine serum, and 1% bovine serum albumin (BSA) to block nonspecific binding sites. The sections were then incubated at 4 °C for 24 h in the primary antiserum diluted 1:4000 in 0.01 M PBS with 0.3% Triton X-100 and 1% BSA. The primary polyclonal antiserum (1:4000) was generated in a rabbit against the *N*-terminal peptide similar to amino acids 2−17 of the rat c-Fos protein in our laboratory and characterized previously.[70] After incubation in primary antiserum, immunoreactivity was detected by means of the avidin−biotin method using diaminobenzidine as chromagen as previously described.[69] The number of c-Fos positive cells were counted by means of light microscopy (20× magnification) using a counting grid (500 $\mu$m × 500 $\mu$m) placed over either the shell of nucleus accumbens (ACCshell), core of nucleus accumbens (ACCcore), or dorsolateral part of the rostral striatum (DLstriatum) (Figure 4) by an observer blind to treatment regimens. The number of c-Fos positive cells was averaged from two adjacent sections of each animal, and statistical analysis was performed on group means ± SEM using a one-way ANOVA with Newman−Keul's posthoc test.

**Acknowledgment.** We thank MIUR−Rome, Italy (PRIN), and NeuroSearch A/S Ballerup, Denmark, for financial support.

**Supporting Information Available:** Multiple sequence alignment of the 7TMs region of bovine rhodopsin, human $\beta_2$-adrenergic receptors, between them and with the 7TMs region modelled of human $D_2$R, $D_3$R, 5-$HT_{1A}$R, 5-$HT_{2A}$R, and 5$HT_{2C}$R, percentage of neutral and protonated form on the aliphatic nitrogen of the

piperazine ring at pH = 7.2 of compounds **5a**−**m** accordingly to apparent p$K_a$ value estimated with ACD/p$K_a$ DB, experimental procedure for the synthesis of compounds **10**−**12**, and elemental analysis data. This material is available free of charge via the Internet at http://pubs.acs.org.

## References


(1) Practice guideline for the treatment of patients with schizophrenia. American Psychiatric Association. *Am. J. Psychiatry* **1997**, *154*, 1−63.

(2) Carlsson, A. The current status of the dopamine hypothesis of schizophrenia. *Neuropsychopharmacology* **1988**, *1*, 179–186.

(3) Meltzer, H. Y. Clinical studies on the mechanism of action of clozapine: the dopamine-serotonin hypothesis of schizophrenia. *Psychopharmacology (Berlin)* **1989**, *99*, S18–S27.

(4) Campbell, M.; Young, P. I.; Bateman, D. N.; Smith, J. M.; Thomas, S. H. The use of atypical antipsychotics in the management of schizophrenia. *Br. J. Clin. Pharmacol.* **1999**, *47*, 13–22.

(5) Koller, E. A.; Doraiswamy, P. M. Olanzapine-associated diabetes mellitus. *Pharmacotherapy* **2002**, *22*, 841–852.

(6) Geddes, J.; Freemantle, N.; Harrison, P.; Bebbington, P. Atypical antipsychotics in the treatment of schizophrenia: systematic overview and meta-regression analysis. *Br. Med. J.* **2000**, *321*, 1371–1376.

(7) McGawin, J. K.; Goa, K. L. Aripiprazole. *CNS Drugs* **2002**, *16*, 779–786.

(8) Buckley, P. F. Aripiprazole: Efficacy and Tolerability Profile of a Novel-Acting Atypical Antipsychotic. *Drugs Today* **2003**, *2*, 145–151.

(9) Butini, S.; Campiani, G.; De Angelis, M.; Fattorusso, C.; Nacci, V.; Fiorini, I. Novel antipsychotic agents: recent advances in the drug treatment of schizophrenia. *Expert Opin. Ther. Patents* **2003**, *13*, 425–448.

(10) Morphy, R.; Rankovic, Z. Designed multiple ligands. An emerging drug discovery paradigm. *J. Med. Chem.* **2005**, *48*, 6523–6543.

(11) Zhong, P.; Yuen, E. Y.; Yan, Z. Modulation of Neuronal Excitability by Serotonin−NMDA Interactions in Prefrontal Cortex. *Mol. Cell. Neurosci.* **2008**, *38*, 290–299.

(12) (a) Mason, S. L.; Reynolds, G. P. Clozapine has submicromolar affinity for 5-$HT_{1A}$ receptors in human brain tissue. *Eur. J. Pharmacol.* **1992**, *221*, 397–398. (b) Elliott, J.; Reynolds, G. P. Agonist-stimulated GTPgamma[$^{35}$S] binding to 5-$HT_{1A}$ receptors in human post-mortem brain. *Eur. J. Pharmacol.* **1999**, *386*, 313–315. (c) Richelson, E.; Souder, T. Binding of antipsychotic drugs to human brain receptors. Focus on newer generation compounds. *Life Sci.* **2000**, *68*, 29–39.

(13) Yoshida, K.; Sugita, T.; Higuchi, H.; Hishikawa, Y. Effect of tandospirone on tardive dyskinesia and parkinsonian symptoms. *Eur. Psychiatry* **1998**, *13*, 421–422.

(14) Christoffersen, C. L.; Meltzer, L. T. Reversal of haloperidol-induced extrapiramidal side effects in cebus monkeys by 8-hydroxy-2-(di-*N*-propylamino)tetralin and its enantiomers. *Neuropsychopharmacology* **1998**, *18*, 399–402.

(15) Millan, M. J. Improving the treatment of schizophrenia: focus on serotonin 5-$HT_{1A}$ receptors. *J. Pharmacol. Exp. Ther.* **2000**, *295*, 853–861.

(16) Marona-Lewicka, D.; Nichols, D. E. Aripiprazole (OPC-14597) fully substitutes for the 5-$HT_{1A}$ receptor agonist LY293284 in the drug discrimination assay in rats. *Psychopharmacology (Berlin)* **2004**, *172*, 415–421.

(17) Jordan, S.; Koprivica, V.; Chen, R.; Tottori, K.; Kikuchi, T.; Altar, C. A. The antipsychotic aripiprazole is a potent, partial agonist at the human 5-$HT_{1A}$ receptor. *Eur. J. Pharmacol.* **2002**, *441*, 137–140.

(18) Mauler, F.; Fahrig, T.; Horvath, E.; Jork, R. Inhibition of evoked glutamate release by the neuroprotective 5-$HT_{1A}$ receptor agonist BAY X 3702 in vitro and in vivo. *Brain Res.* **2001**, *888*, 150–157.

(19) Meltzer, H. Y.; Sumiyoshi, T. Does stimulation of 5-$HT_{1A}$ receptors improve cognition in schizophrenia. *Behav. Brain Res.* **2008**, *195*, 98–102.

(20) (a) Schwartz, J. C.; Diaz, J.; Pilon, C.; Sokoloff, P. Possible implications of the dopamine $D_3$ receptor in schizophrenia and in antipsychotic drug actions. *Brain Res. Brain Res. Rev.* **2000**, *31*, 277–287. (b) Joyce, J. N.; Millan, M. J. Dopamine $D_3$ receptor antagonists as therapeutic agents. *Drug Discovery Today* **2005**, *10*, 917–925.

(21) Millan, M. J.; Loiseau, F.; Dekeyne, A.; Gobert, A.; Flik, G.; Cremers, T. I.; Rivet, J. M.; Sicard, D.; Billiras, R.; Brocco, M. S33138 (*N*-[4-[2-[(3a*S*,9b*R*)-8-cyano-1,3a,4,9b-tetrahydro[1] benzopyrano[3,4-*c*]pyrrol-2(3*H*)-yl)-ethyl]phenyl-acetamide), a preferential dopamine $D_3$ versus $D_2$ receptor antagonist and potential antipsychotic agent: III. Actions in models of therapeutic activity and induction of side effects. *J. Pharmacol. Exp. Ther.* **2008**, *324*, 1212–1226.

(22) (a) Campiani, G.; Nacci, V.; Bechelli, S.; Ciani, S. M.; Garofalo, A.; Fiorini, I.; Wikstrom, H.; de Boer, P.; Liao, Y.; Tepper, P. G.; Cagnotto, A.; Mennini, T. New Antipsychotic Agents with Serotonin and Dopamine Antagonist Properties Based on a Pyrrolo[2,1-*b*][1,3]benzothiazepine Structure. *J. Med. Chem.* **1998**, *41*, 3763–3772. (b) Campiani, G.; Butini, S.; Gemma, S.; Nacci, V.; Fattorusso, C.; Catalanotti, B.; Giorgi, G.; Cagnotto, A.; Goegan, M.; Mennini, T.; Minetti, P.; Di Cesare, M. A.; Mastroianni, D.; Scafetta, N.; Galletti, B.; Stasi, M. A.; Castorina, M.; Pacifici, L.; Ghirardi, O.; Tinti, O.; Carminati, P. Pyrrolo[1,3]benzothiazepine atypical antipsychotic agents. Synthesis, structure−activity relationships, molecular-modelling, and biological studies. *J. Med. Chem.* **2002**, *45*, 344–359. (c) Campiani, G.; Butini, S.; Fattorusso, C.; Catalanotti, B.; Gemma, S.; Nacci, V.; Morelli, E.; Cagnotto, A.; Mereghetti, I.; Mennini, T.; Carli, M.; Minetti, P.; Di Cesare, M. A.; Mastroianni, D.; Scafetta, N.; Galletti, B.; Stasi, M. A.; Castorina, M.; Pacifici, L.; Vertechy, M.; Di Serio, S.; Ghirardi, O.; Tinti, O.; Carminati, P. Pyrrolo[1,3]benzothiazepine-based serotonin and dopamine receptor antagonists. Molecular modeling, further structure−activity relationship studies, and identification of novel atypical antipsychotic agents. *J. Med. Chem.* **2004**, *47*, 143–157. (d) Campiani, G.; Butini, S.; Fattorusso, C.; Trotta, F.; Gemma, S.; Catalanotti, B.; Nacci, V.; Fiorini, I.; Cagnotto, A.; Mereghetti, I.; Mennini, T.; Minetti, P.; Di Cesare, M. A.; Stasi, M. A.; Di Serio, S.; Ghirardi, O.; Tinti, O.; Carminati, P. Novel atypical antipsychotic agents: rational design, an efficient palladium-catalyzed route, and pharmacological studies. *J. Med. Chem.* **2005**, *48*, 1705–1708.

(23) Campiani, G.; Butini, S.; Trotta, F.; Fattorusso, C.; Catalanotti, B.; Aiello, F.; Gemma, S.; Nacci, V.; Novellino, E.; Stark, J. A.; Cagnotto, A.; Fumagalli, E.; Carnovali, F.; Cervo, L.; Mennini, T. Synthesis and pharmacological evaluation of potent and highly selective $D_3$ receptor ligands: inhibition of cocaine-seeking behavior and the role of dopamine $D_3$/$D_2$ receptors. *J. Med. Chem.* **2003**, *46*, 3822–3839.

(24) Suzuki, H.; Gyoutoku, H.; Yokoo, H.; Shinba, M.; Sato, Y.; Yamada, H.; Murakami, Y. Unexpected formation of quinolone derivatives in Reissert indole synthesis. *Synlett* **2000**, *8*, 1196–1199.

(25) Rajur, S. B.; Merwade, A. Y.; Flendi, S. B.; Basanagoudar, I. D. Synthesis of 1,2,3,4-tetrahydropyrazino[1,2-*a*]indoles and ethyl 1-(2-amino-ethyl)indole-2-carboxylates. *Indian J. Chem.* **1989**, *28B*, 1065–1068.

(26) Repke, D. B., III. Synthesis of 5-methoxy-and 5-hydroxy-1,2,3,4-tetrahydro-9*H*-pyrido[3,4-*b*]indoles. *J. Heterocycl. Chem.* **1982**, *19*, 845–848.

(27) Sugimoto, O.; Mori, M.; Moriya, K.; Tanji, K. Application of phosphonium salts to the reactions of various kinds of amides. *Helv. Chim. Acta* **2001**, *84*, 1112–1118.

(28) Robertson, A. A. B.; Botting, N. P. Synthesis of deuterium labelled desulfoglucosinolates as internal standards for LC-MS analysis. *Tetrahedron* **1999**, *55*, 13269–13284.

(29) GPCR alignments; www.bioinfo-pharma.u-strasbg.fr/gpcrdb/jss.html.

(30) Terakita, A. The opsins. *Genome Biol.* **2005**, *6*, 213.

(31) Gether, U.; Kobilka, B. K. G protein-coupled receptors. II. Mechanism of agonist activation. *J. Biol. Chem.* **1998**, *273*, 17979–17982.

(32) Ballesteros, J. A.; Jensen, A. D.; Liapakis, G.; Rasmussen, S. G.; Shi, L.; Gether, U.; Javitch, J. A. Activation of the beta 2-adrenergic receptor involves disruption of an ionic lock between the cytoplasmic ends of transmembrane segments 3 and 6. *J. Biol. Chem.* **2001**, *276*, 29171–29177.

(33) Shapiro, D. A.; Kristiansen, K.; Weiner, D. M.; Kroeze, W. K.; Roth, B. L. Evidence for a model of agonist-induced activation of 5-hydroxytryptamine 2A serotonin receptors that involves the disruption of a strong ionic interaction between helices 3 and 6. *J. Biol. Chem.* **2002**, *277*, 11441–11449.

(34) Schwartz, T. W.; Frimurer, T. M.; Holst, B.; Rosenkilde, M. M.; Elling, C. E. Molecular mechanism of 7TM receptor activation−a global toggle switch model. *Annu. Rev. Pharmacol. Toxicol.* **2006**, *46*, 481–519.

(35) Shi, L.; Javitch, J. A. The binding site of aminergic G protein-coupled receptors: the transmembrane segments and second extracellular loop. *Annu. Rev. Pharmacol. Toxicol.* **2002**, *42*, 437–467.

(36) Javitch, J. A.; Ballesteros, J. A.; Weinstein, H.; Chen, J. A cluster of aromatic residues in the sixth membrane-spanning segment of the dopamine D2 receptor is accessible in the binding-site crevice. *Biochemistry* **1998**, *37*, 998–1006.

(37) Rasmussen, S. G.; Choi, H. J.; Rosenbaum, D. M.; Kobilka, T. S.; Thian, F. S.; Edwards, P. C.; Burghammer, M.; Ratnala, V. R.; Sanishvili, R.; Fischetti, R. F.; Schertler, G. F.; Weis, W. I.; Kobilka, B. K. Crystal structure of the human beta2 adrenergic G-protein-coupled receptor. *Nature* **2007**, *450*, 383–387.

(38) Cherezov, V.; Rosenbaum, D. M.; Hanson, M. A.; Rasmussen, S. G.; Thian, F. S.; Kobilka, T. S.; Choi, H. J.; Kuhn, P.; Weis, W. I.; Kobilka, B. K.; Stevens, R. C. High-resolution crystal structure of an engineered human beta2-adrenergic G protein-coupled receptor. *Science* **2007**, *318*, 1258–1265.

(39) Rosenbaum, D. M.; Cherezov, V.; Hanson, M. A.; Rasmussen, S. G.; Thian, F. S.; Kobilka, T. S.; Choi, H. J.; Yao, X. J.; Weis, W. I.;

Stevens, R. C.; Kobilka, B. K. GPCR engineering yields high-resolution structural insights into beta2-adrenergic receptor function. *Science* **2007**, *318*, 1266–1273.
(40) Kalani, M. Y.; Vaidehi, N.; Hall, S. E.; Trabanino, R. J.; Freddolino, P. L.; Kalani, M. A.; Floriano, W. B.; Kam, V. W.; Goddard, W. A., 3rd. The predicted 3D structure of the human D2 dopamine receptor and the binding site and binding affinities for agonists and antagonists. *Proc. Natl. Acad. Sci. U.S.A.* **2004**, *101*, 3815–3820.
(41) Roth, B. L.; Shoham, M.; Choudhary, M. S.; Khan, N. Identification of conserved aromatic residues essential for agonist binding and second messenger production at 5-hydroxytryptamine2A receptors. *Mol. Pharmacol.* **1997**, *52*, 259–266.
(42) Boeckler, F.; Gmeiner, P. The structural evolution of dopamine $D_3$ receptor ligands: structure−activity relationships and selected neuropharmacological aspects. *Pharmacol. Ther.* **2006**, *112*, 281–333.
(43) Boess, F. G., Jr.; Meyer, V.; Zwingelstein, C.; Sleight, A. J. Interaction of tryptamine and ergoline compounds with threonine 196 in the ligand binding site of the 5-hydroxytryptamine$_6$ receptor. *Mol. Pharmacol.* **1997**, *52*, 515–523.
(44) Shapiro, D. A.; Kristiansen, K.; Kroeze, W. K.; Roth, B. L. Differential modes of agonist binding to 5-hydroxytryptamine(2A) serotonin receptors revealed by mutation and molecular modeling of conserved residues in transmembrane region 5. *Mol. Pharmacol.* **2000**, *58*, 877–886.
(45) Johnson, M. P.; Loncharich, R. J.; Baez, M.; Nelson, D. L. Species variations in transmembrane region V of the 5-hydroxytryptamine type 2A receptor alter the structure−activity relationship of certain ergolines and tryptamines. *Mol. Pharmacol.* **1994**, *45*, 277–286.
(46) Almaula, N.; Ebersole, B. J.; Ballesteros, J. A.; Weinstein, H.; Sealfon, S. C. Contribution of a helix 5 locus to selectivity of hallucinogenic and nonhallucinogenic ligands for the human 5-hydroxytryptamine$_{2A}$ and 5-hydroxytryptamine$_{2C}$ receptors: direct and indirect effects on ligand affinity mediated by the same locus. *Mol. Pharmacol.* **1996**, *50*, 34–42.
(47) Recanatini, M.; Cavalli, A.; Masetti, M. Modeling hERG and its Interactions with Drugs: Recent Advances in Light of Current Potassium Channel Simulations. *ChemMedChem.* **2008**, *3*, 523–535.
(48) Stansfeld, P. J.; Gedeck, P.; Gosling, M.; Cox, B.; Mitcheson, J. S.; Sutcliffe, M. J. Drug block of the hERG potassium channel: insight from modelling. *Proteins* **2007**, *68*, 568–580.
(49) Farid, R.; Day, T.; Friesner, R. A.; Pearlstein, R. A. New insights about hERG blockade obtained from protein modeling, potential energy mapping, and docking studies. *Bioorg. Med. Chem.* **2006**, *14*, 3160–3173.
(50) Kamiya, K.; Niwa, R.; Mitcheson, J. S.; Sanguinetti, M. C. Molecular determinants of hERG channel block. *Mol. Pharmacol.* **2006**, *69*, 1709–1716.
(51) Myokai, T.; Ryu, S.; Shimizu, H.; Oiki, S. Topological mapping of the asymmetric drug binding to the human ether-à-go-go-related gene product (hERG) potassium channel by use of tandem dimers. *Mol. Pharmacol.* **2008**, *73*, 1643–1651.
(52) Pearlstein, R. A.; Vaz, R. J.; Kang, J.; Chen, X. L.; Preobrazhenskaya, M.; Shchekotikhin, A. E.; Korolev, A. M.; Lysenkova, L. N.; Miroshnikova, O. V.; Hendrix, J.; Rampe, D. Characterization of hERG potassium channel inhibition using CoMSiA 3D QSAR and homology modeling approaches. *Bioorg. Med. Chem. Lett.* **2003**, *13*, 1829–1835.
(53) Cavalli, A.; Poluzzi, E.; De Ponti, F.; Recanatini, M. Toward a pharmacophore for drugs inducing the long QT syndrome: insights from a CoMFA study of hERG K(+) channel blockers. *J. Med. Chem.* **2002**, *45*, 3844–3853.
(54) Ichikawa, J.; Ishii, H.; Bonaccorso, S.; Fowler, W. L.; O'Laughlin, I. A.; Meltzer, H. Y. 5-$HT_{2a}$ and $D_2$ receptor blockade increases cortical DA release via 5-$HT_{1a}$ receptor activation: a possible mechanism of atypical antipsychotic-induced cortical dopamine release. *J. Neurochem.* **2001**, *76*, 1521–1531.
(55) (a) Maurel-Remy, S.; Bervoets, K.; Millan, M. J. Blockade of phencyclidine-induced hyperlocomotion by clozapine and MDL 100907 in rats reflects antagonism of 5-$HT_{2A}$ receptors. *Eur. J. Pharmacol.* **1995**, *280*, R9–R11. (b) Gleason, S. D.; Shannon, H. E. Blockade of phencyclidine-induced hyperlocomotion by olanzapine, clozapine and serotonin receptor subtype selective antagonists in mice. *Psychopharmacology (Berlin)* **1997**, *129*, 79–84.
(56) (a) Deutch, A. Y.; Lee, M. C.; Iadarola, M. J. Regionally specific effects of atypical antipsychotic drugs on striatal fos expression: the nucleus accumbens shell as a locus of antipsychotic action. *Mol. Cell. Neurosci.* **1992**, *3*, 332–341. (b) Robertson, G. S.; Fibiger, H. C. Neuroleptics increase c-fos expression in the forebrain: contrasting effects of haloperidol and clozapine. *Neuroscience* **1992**, *46*, 315–328.
(57) Tremblay, P. O.; Gervais, J.; Rouillard, C. Modification of haloperidol-induced pattern of c-fos expression by serotonin agonists. *Eur. J. Neurosci.* **1998**, *10*, 3546–3555.
(58) Robertson, G. S.; Matsumura, H.; Fibiger, H. C. Induction Patterns of Fos-Like Immunoreactivity in the Forebrain as Predictors of Atypical Antipsychotic Activity. *J. Pharmacol. Exp. Ther.* **1994**, *271*, 1058–1066.
(59) Sumner, B. E.; Cruise, L. A.; Slattery, D. A.; Hill, D. R.; Shahid, M.; Henry, B. Testing the validity of c-fos expression profiling to aid the therapeutic classification of psychoactive drugs. *Psychopharmacology (Berlin)* **2004**, *171*, 306–321.
(60) Belfield, A. J.; Brown, G. R.; Foubister, A. J.; Ratcliffe, P. D. Synthesis of *meta*-substituted aniline derivatives by nucleophilic substitution. *Tetrahedron* **1999**, *55*, 13285–13300.
(61) Butini, S.; Campiani, G.; Borriello, M.; Gemma, S.; Panico, A.; Persico, M.; Catalanotti, B.; Ros, S.; Brindisi, M.; Agnusdei, M.; Fiorini, I.; Nacci, V.; Novellino, E.; Belinskaya, T.; Saxena, A.; Fattorusso, C. Exploiting Protein Fluctuations at the Active-Site Gorge of Human Cholinesterases: Further Optimization of the Design Strategy to Develop Extremely Potent Inhibitors. *J. Med. Chem.* **2008**, *51*, 3154–3170.
(62) Ding, H. Q.; Karasawa, N.; Goddard, W. A III atomic level simulations on a million particles: the cell multipole method for Coulomb and London nonbond interactions. *J. Chem. Phys.* **1992**, *97*, 4309–4315.
(63) Dauber-Osguthorpe, P.; Roberts, V. A.; Osguthorpe, D. J.; Wolff, J.; Genest, M.; Hagler, A. T. Structure and energetics of ligand binding to proteins: *Escherichia coli* dihydrofolate reductase-trimethoprim, a drug-receptor system. *Proteins* **1988**, *4*, 31–47.
(64) Maple, J. R.; Hwang, M. J.; Stockfisch, T. P.; Dinur, U.; Waldman, M.; Ewig, C. S.; Hagler, A. T. Derivation of class II force fields. I. Methodology and quantum force field for the alkyl functional group and alkane molecules. *J. Comput. Chem.* **1994**, *15*, 162–182.
(65) Stewart, J. P. MOPAC; Stewart Computational Chemistry: Colorado Springs, CO, 2007; http://OpenMOPAC.net.
(66) Dini, S.; Caselli, G. F.; Ferrari, M. P.; Giani, R.; Clavenna, G. Heterogenity of [$^3$H]-mepyramine binding sites in guinea pig cerebellum and lung. *Agents Actions* **1991**, *33*, 181–184.
(67) DeLean, K. W.; Munson, P. J.; Rodbard, D. Simultaneous analysis of families of sigmoidal curves: application to bioassay, radioligand assay and physiological dose-response curves. *Am. J. Physiol.* **1978**, *235*, E97–E102.
(68) Cheng, Y.; Prusoff, W. H. Relationship between the inhibition constant (*K*1) and the concentration of inhibitor which causes 50% inhibition ($IC_{50}$) of an enzymatic reaction. *Biochem. Pharmacol.* **1973**, *22*, 3099–3108.
(69) Hansen, H. H.; Timmermann, D. B.; Peters, D.; Walters, C.; Damaj, M. I.; Mikkelsen, J. D. Alpha-7 nicotinic acetylcholine receptor agonists selectively activate limbic regions of the rat forebrain: an effect similar to antipsychotics. *J. Neurosci. Res.* **2007**, *85*, 1810–1818.
(70) Mikkelsen, J. D.; Vrang, N.; Mrosovsky, N. Expression of Fos in the circadian system following nonphotic stimulation. *Brain Res. Bull.* **1998**, *47*, 367–376.

JM800689G